PLOS BIOLOGY

Individualistic reward-seeking strategies that predict response to nicotine emerge among isogenic male mice living in a micro-society

Sophie L. Fayad[1,2☯], Lauren M. Reynolds[1,2☯], Nicolas Torquet[1], Stefania Tolu[1], Sarah Mondoloni[1], Claire Nguyen[1], Amy Siriphanh[1], Robin Justo[1,2], Steve Didienne[1,2], Nicolas Debray[2], Cécile Viollet[2], Louis Raynaud[2], Yasmine Layadi[2], Coralie Fouquet[1], Bernadette Hannesse[1], Ana-Marta Capaz[3], Thomas Topilko[3], Nicolas Renier[3], Alexandre Mourot[1,2], Fabio Marti[1,2], Philippe Faure[1,2]*

1 Sorbonne University, INSERM, CNRS UMR8246, Neuroscience Paris Seine—Institut de Biologie Paris Seine (NPS—IBPS), Paris, France, 2 ESPCI Paris, PSL Research University, Brain Plasticity laboratory, CNRS UMR8249, Paris, France, 3 Sorbonne University, ICM Institut du Cerveau et de la Moelle Epinière, Laboratoire de Plasticité Structurale INSERM U1127, CNRS UMR7225, Paris, France

☯ These authors contributed equally to this work.
* phfaure@gmail.com

Abstract

Individual animals differ in their traits and preferences, which shape their social interactions, survival, and susceptibility to disease, including addiction. Nicotine use is highly heterogenous and has been linked to the expression of personality traits. Although these relationships are well documented, we have limited understanding of the neurophysiological mechanisms that give rise to distinct behavioral profiles and their connection to nicotine susceptibility. To address this question, we conducted a study using a semi-natural and social environment called "Souris-City" to observe the long-term behavior of individual male mice. Souris-City provided both a communal living area and a separate test area where mice engaged in a reward-seeking task isolated from their peers. Mice developed individualistic reward-seeking strategies when choosing between water and sucrose in the test compartment, which, in turn, predicted how they adapted to the introduction of nicotine as a reinforcer. Moreover, the profiles mice developed while isolated in the test area correlated with their behavior within the social environment, linking decision-making strategies to the expression of behavioral traits. Neurophysiological markers of adaptability within the dopamine system were apparent upon nicotine challenge and were associated with specific profiles. Our findings suggest that environmental adaptations influence behavioral traits and sensitivity to nicotine by acting on dopaminergic reactivity in the face of nicotine exposure, potentially contributing to addiction susceptibility. These results further emphasize the importance of understanding interindividual variability in behavior to gain insight into the mechanisms of decision-making and addiction.

Competing interests: The authors have declared that no competing interests exist.

Abbreviations: nAChR, nicotinic acetylcholine receptor; RFID, radio frequency identification; RL, reinforcement learning; RPE, reward prediction error; VTA, ventral tegmental area.

Introduction

Interindividual behavioral variability refers to consistent differences in behavior between members of a population or group. This variability is observed in both humans and mice [1–7]. It is seen not only in how individuals adapt to their environment but also in their susceptibility to diseases. This is particularly evident in the context of addiction, as not all individuals will develop drug abuse despite equal exposure to a given psychoactive substance [8].

Capturing and interpreting interindividual variability in animal experiments can be challenging [5,9–12]. Longitudinal and complex quantification of individual behaviors is necessary, alongside careful consideration of experimental design. We studied resource foraging, a very important aspect of animal life and a fundamental focus of neuroeconomic studies [13–15]. Our behavioral paradigm utilized a closed-economy setup [16–18], where food and liquids are always present, 24 h a day. Animals live in groups (approximately 10 mice) representing a "micro-society" [5,9,11]. Rodents, known for their social nature, exhibit a range of interactive behaviors—such as physical contact, vocal communication, aggression, social recognition—that can be considered as hallmarks of sociability [19]. Importantly, when mice live in microsocieties within a closed and enriched naturalistic environment, strong and stable interindividual variability in behavior related to foraging, decision-making, and exploration emerges, even among isogenic animals [5,9].

Behavioral trait components of decision-making, such as impulsivity, exploration, or novelty seeking, are thought to predict vulnerability to drugs of abuse [20,21]. While these traits have indeed been linked with smoking and addiction to nicotine in humans and animal models, certain traits, like impulsivity or sensation-seeking, have been more strongly associated with initial nicotine sensitivity [22–24], suggesting that they are a measure of vulnerability to nicotine. However, whether the processes leading to nicotine addiction and the mechanisms of decision-making share mechanistic underpinnings remains elusive. Altered dopamine circuit function is a promising mechanistic candidate [10,25], as dopaminergic signaling is implicated in decision-making, in social behaviors, and in nicotine addiction, where the initial stage critically involves activation of mesolimbic dopamine neurons [26–28]. As such, investigating variations in nicotinic control over the DA system represents a particularly promising avenue for linking interindividual differences in decision-making and vulnerability to nicotine. Nicotine initiates reinforcement by increasing the firing rate and bursting activity of DA neurons through direct actions on nicotinic acetylcholine receptors (nAChRs), a family of pentameric ligand-gated ion channels with 12 different types of subunits expressed in the mammalian brain. It has been shown that the transition between tonic and phasic activity of DA neurons induced by nicotine is essential for the reinforcement [29,30], and that the expression of nicotine-sensitive nAChR subtypes in the VTA is necessary for both the cellular and behavioral effects of nicotine [29,31–33]. Under nicotine-free conditions, nAChRs in the VTA are also key modulators of DA activity through basal cholinergic signaling, and they regulate specific aspects of reward-seeking behaviors, in particular, exploration and reaction to uncertainty [34,35]. Environmental manipulations that alter nAChR-mediated control of DA neurons may therefore lead to changes in downstream behaviors. For example, nicotine exposure modifies exploratory behavior [36,37], by increasing, in mice, DA neuron activity and biasing individual strategies toward reduced exploration [38]. In addition, specific social contexts (i.e., repeated aggression) have been shown to induce a marked remodeling of the dopaminergic and nicotinic system, leading to increased VTA DA neuron activity [39,40], social aversion, and modified nicotine response [41]. This crosstalk at the level of the DA system between responses to drugs and modifications of decision-making could explain the observed correlation between novelty seeking and susceptibility to nicotine.

Here, we aim to demonstrate whether the way individuals adapt to their environment is related to the nicotinic modulation of their DA networks, and, consequently, whether this relationship defines their initial sensitivity to nicotine, a critical element that may define susceptibility to nicotine addiction [42,43]. For that purpose, we used a habitat called "Souris-City" that combines a large social environment where mice live together with a modular testing platform where animals individually perform cognitive tests. In this environment, mice have individual access to water by performing a specific task in a T-maze, while social, circadian, and cognitive behaviors are continuously monitored over time using multiple sensors [5].

Results

Souris-City: Continuous tracking of individual mice living within a micro-society

Souris-City is a semi-naturalistic environment composed of a large and complex housing space in which groups of mice (N = 32 groups) live together (5 to 10 male mice per group, mean = 8.8) for extended periods of time (1 to 3 months) and are able to express sophisticated social and non-social behaviors. The environment includes a test-area (individual zone), separated from the main environment (social zone) by a gate which selectively controls the passage of mice, one at a time, based on a radio frequency identification (RFID) (Fig 1A). The test area consists of a T-maze leading to 2 drinking areas at the end of the left and right arms, where mice can perform a self-initiated cognitive task individually, spontaneously, and isolated from their cage mates. Thus, Souris-City associates a zone for individual liquid consumption and a social zone (the main cage) where food is always available. The experimental paradigm involves several consecutive periods with modified rules regarding access to and the nature of the liquids (Fig 1B). During a 1-week habituation period, mice explore Souris-City with free access to the T-maze. The gate is always open, so several mice can access the T-maze simultaneously, and water is delivered from both sides. In the second period (WW, mean duration = 9.5 days, n = 281 mice), mice continue to have water on both sides of the T-maze, but its access is now restricted by the gate so that mice can only enter the T-maze one at a time. Choice is restricted so that if the animal chooses one side, access to the opposite arm closes. During the subsequent weeks (WS, mean duration = 25.2 days, n = 281 mice), water and a 5% sucrose solution are respectively delivered on each side of the gate-restricted T-maze, thus introducing a choice (choosing left or right) which modifies the reward associated with liquid consumption. The positions of water and sucrose bottles are swapped twice a week, which allows for the mice to stabilize their choice. Overall, in 32 experiments (or groups of mice) in the water-sucrose (WS) test period, the behavior of 281 mice and more than 100,000 choices were analyzed.

The data obtained in Souris-City are based on the tracking of animals implanted subcutaneously with RFID chips and detected by antennae placed throughout the floor and the tubes connecting the different compartments of the environment (see Methods). Mice have free access to a nest compartment (N), a food compartment (F), a central compartment that provides access to all other compartments (C), the stair (S), and finally the T-maze (T). These subdivisions allow animal trajectories in Souris-City to be represented as a sequence of residency times within a compartment and transitions between sub-compartments [35,44]. The circadian rhythm of the group emerged from the measurement of pooled activity estimated from RFID detection at the level of the transition tubes during the WS period (Fig 1C). As expected, the mice are more active (and therefore more frequently detected moving between sub-compartments) during the dark phase (7 PM to 7 AM) than during the light phase (7 AM to 7 PM). The time spent by mice in a given compartment during the WS period varied between
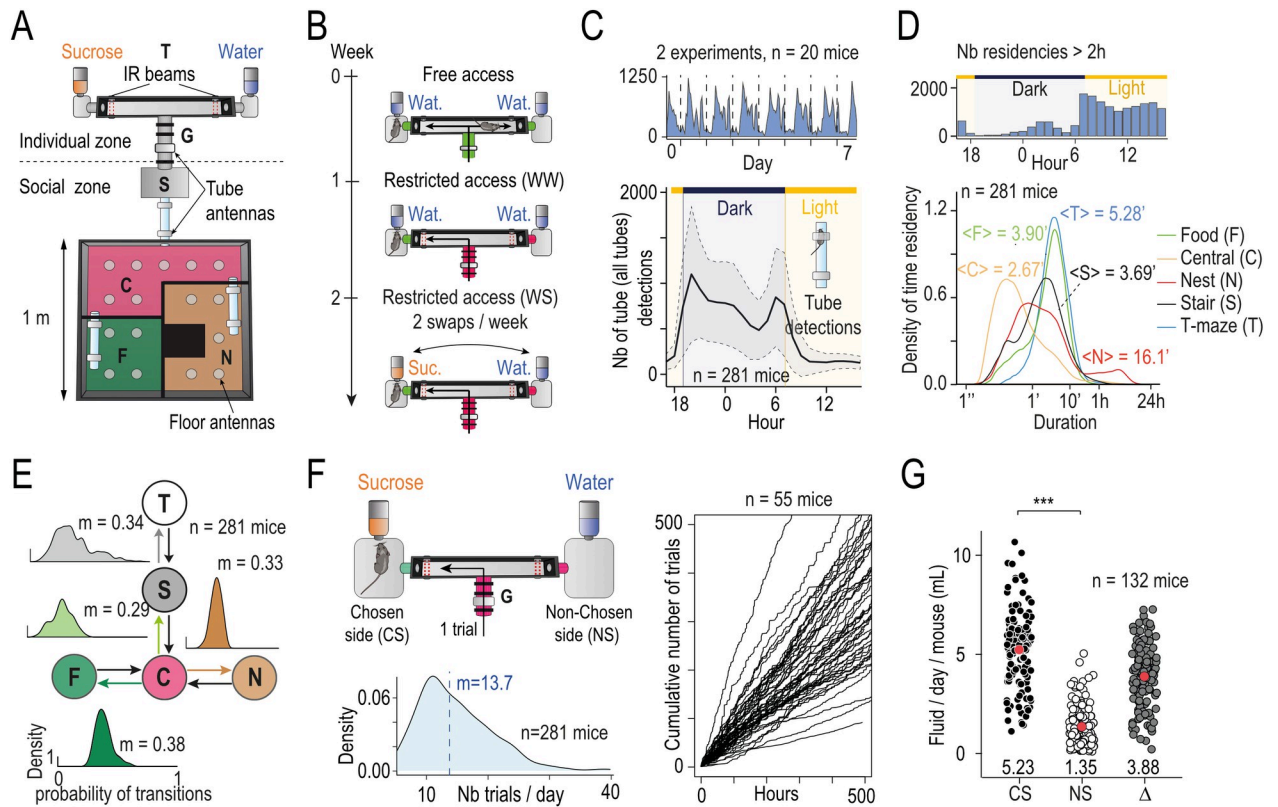
Fig 1. Longitudinal profiling of individual and group behavior among mouse micro-societies within Souris-City. (**A**) Souris-City is divided into 2 main parts: a social zone and a test zone. The social zone includes a square cage measuring 1 m × 1 m, which is further divided into 4 compartments: the nest (N), the food (F) area, where mice have unrestricted access to food, and the central (C) zone that serves as a hub, connecting the social compartments with a stair (S) leading to the test zone. The test zone is a T-maze, which is separated from the stair by a controlled access gate (G). Mice are tagged with RFID chips and detected using floor-mounted circular or tube-shaped RFID antennae, which connect compartments of SC to capture transitions between zones. Two infrared beams (red dashed lines) are used to detect which arm mice choose in the T-maze. (**B**) The experimental paradigm involves several consecutive sessions with modified rules regarding access to the maze and the nature of the liquids available at each arm. During the free access period (top), mice are allowed unrestricted access to the T-maze for 1 week. The gate remains open, allowing multiple mice to enter the T-maze simultaneously, and water is detected from both sides. In a second step (middle), mice choose between water on both sides of the T-maze (WW, mean duration = 9.5 days); however, access to the T-maze is restricted by the gate, and mice may only enter the T-maze one at a time. Choice is restricted so that if the animal chooses one side, access to the opposite arm is closed. Finally, water and 5% sucrose solution (bottom, WS, mean duration = 25.2 days) are respectively delivered at each side of the gate-restricted T-maze, introducing a choice (choosing left or right, choosing water or sucrose). The positions of the water and sucrose bottles are then swapped twice a week. (**C**) Overall activity of mice captured from their movement in Souris-City reflects their circadian rhythm. (Top) Tube detection events for 8 consecutive days ($n = 20$ mice, 2 group of 10 in parallel). (Bottom) Daily tube detection events per hours averaged for all mice (mean ± SEM, $n = 281$). (**D**) Residency time in each sub-compartment can be captured by floor antennae. (*Top*) Histogram (bin per hour) of the number of residencies in the nest zone longer than 2 h. (*Bottom*) Density of residency time in each sub-compartment (log-scale, bandwidth = 0.1), with indicated mean value. (**E**) Tube antennae provide information about the movement of mice between sub-compartments. Flow diagram of all possible transitions between sub-compartment, density graph above each transition indicates the distribution of conditional transition probability among the $n = 281$ mice, with indicated median value. (**F**) (Left) Distribution of mean number of T-maze entries per day for $n = 281$ mice in the SW session. Vertical dashed line indicates mean value. (Right) Cumulative number of T-maze entries per hours after the beginning of the SW session for $n = 55$ mice (6 experiments). (**G**) Estimation of daily consumption on a subpart of the experiment ($n = 132$ mice, see text) during SW session: Mean daily fluid change per animal distinguishing the chosen side (CS) from the non-selected side (NS) and the difference between the two (Δ) (pairwise comparisons using Wilcoxon rank sum test with continuity correction and Holm p-value adjustment correction, $n = 132$ mice). Data can be found here https://zenodo.org/api/records/13374058/draft/files/Fig 1G.csv/content. Data are represented as mean ± SEM. ns $p > 0.05$, ** $p < 0.01$, *** $p < 0.001$.

https://doi.org/10.1371/journal.pbio.3002850.g001

tens of seconds to hours, with the shortest visits, mainly found in the central compartment, corresponding to transition episodes (Fig 1D, bottom). Time residency in the nest sub-compartment shows a bimodal distribution, with the longest occupancies observed in the environment lasting more than 2 h. The distribution of long occupancy episodes, which took place mainly in the nest compartment, shows that they occurred mostly during the light period

([Fig 1D](#), top), thus they can be interpreted as sleeping episodes. The distribution of transition probabilities from one compartment to another ([Fig 1E](#)) reveals a preponderance of transitions from the central to the food compartment (median = 38%) over transitions from the central towards the nest compartment (33%, Wilcoxon signed rank test $p < 2.2e\text{-}16$) or towards the stair (29%, Wilcoxon signed rank test $p < 2.2e\text{-}16$). Furthermore, when animals are in the stair, their probability of entering the T-maze is only 34%. This relatively low rate reflects the fact that animals enter the stair without necessarily succeeding to enter the T-maze, and then return to the main environment. Mice enter the T-maze an average of 14.7 times per day during the WS period ([Fig 1F](#), left); however, the distribution is skewed with a median at 13.7 and a peak at 11 times per day and a long tail indicating that some mice can enter more than 30 times per day. Interindividual variability in the number of entries is also illustrated by the divergence in the cumulative number of trials over time ([Fig 1F](#), right, example of $n = 55$ individual), which showed stability and consistency in the temporal frequency of T-maze entries. In restricted access sessions, when a mouse chooses one side the access to the bottle on the other, non-chosen, side is closed, so that the mouse has access to only the bottle on the chosen side. The mouse will only be able to access the bottle on the non-chosen side if it leaves the T-maze and returns for another trial, which will reopen access to both bottles, as well as reopening access for other mice to enter. In half of the experiments (16/32 corresponding to $n = 132$ animals), fluid consumption was estimated for each trial (i.e., each passage of a mouse in the T-maze). By comparing the average difference in liquid change between the chosen side and the non-chosen side per day and per animal ([Fig 1G](#), $n = 132$), we find a significant difference in the amount of liquid dispensed depending on the arm chosen. We thus estimate the consumption of the animals by subtracting the loss of liquid measured by the system in the non-chosen side (resulting from evaporation, noise, etc.) from the change in fluid volume measured from the bottle in the chosen side, which results in an average consumption of approximately 3.9 ml per day per mouse ([Fig 1G](#)). These first analyses describe a set of average behaviors, accessible from the analysis of events captured by RFID antennae or consumption sensors. They begin to reveal an organization of behaviors with important variations in their expression depending on the individual mouse.

Multidimensional analysis of reward-seeking behavior reveals that mice adopt idiosyncratic strategies in the T-maze

In the T-maze, mice ($n = 281$) voluntarily performed a relatively simple decision-making task: whether to make a left or right turn to access a liquid reward. In the WS test sessions, one drinking area at the end of one of the T-maze arms contains water, and the other contains a sucrose solution. Each entrance into the T-maze, and the subsequent choice of which side to access, is considered a trial ([Fig 2A](#), top). The sides of the sucrose and water bottles are swapped every 3 to 4 days, with each swap defining the beginning of a new session. The behavior of the mice in the T-maze was assessed by 5 variables that quantify the animals' choice across different time scales throughout the entire WS experimental period. The level of global switching is estimated by the variable *Switch*, which takes all WS sessions into account and gives an overview of the probability of choosing of one side compared to the other. This probability is renormalized so that 100% corresponds to an equivalent number of visits to both sides, while 0 corresponds to an individual who visits only one side. The variables *SwWat* and *SwSuc* evaluate the choices of the animals at the trial level (i.e., going left or right). They represent the probability of switching sides if the previous choice was water or sucrose, respectively. Finally, the *Pref* and *SideBias* variables assess sucrose preference (probability of sucrose choice) and side bias (probability of choices on one side) by comparing the choices between each session
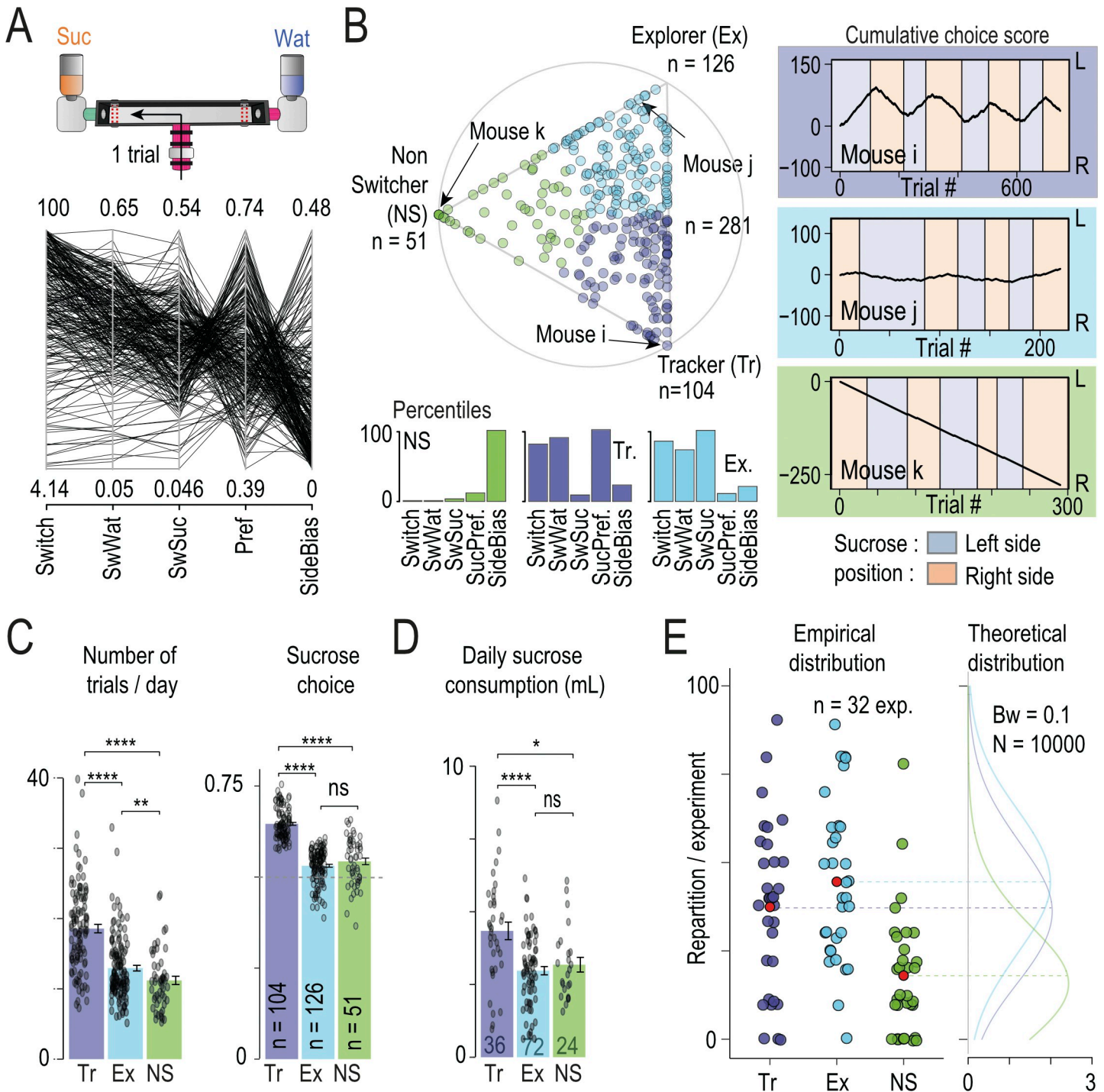
Fig 2. Mice exhibit interindividual differences in choice strategies in the T-maze. (A) Top: one trial is considered to be one choice between left or right side in the T-maze. Bottom: Value of the 5 parameters that describe mice sequence of choice in the T-maze during SW sessions ($n = 281$ mice): the level of global switching (*Switch*), the probability of switching sides if the previous choice was water (*SwWat*) or sucrose (*SwSuc*), the preference (*Pref*) and side bias (*SideBias*) on each session. Top and bottom value correspond to the min (bottom) and max (top) value for each parameter. (B) Archetypal analysis of the choice strategies based on the 5-dimensional data space. Top: Visualization of the α coefficients using a ternary plot. Each point represents the projection of an individual ($n = 281$ mice) onto the plane defined by a triangle where the 3 apices represent the 3 archetypes: Tracker (Tr, purple), Explorer (Ex, blue), and non-Switcher (NS, green). Points are color-coded according to their proximity to the archetypes. Bottom: Histograms showing the 3 archetypes' percentiles for each choice parameter. Right: Examples of 3 sequences of choice made by 3 mice close to the archetype. Sucrose position alternates across sessions between the left (light purple) and the right (light orange) side. Cumulated choices across trials are calculated with a positive (+1) or negative (−1) increment when the left or right side is chosen, respectively. The mouse i, j, k (from top to bottom corresponds respectively to a Tr, Exp and NS profile (see their projection in the ternary plot). (C) Number of trials per days (left) and percentage of sucrose side choice (right) for the 3 archetypes (pairwise Wilcoxon tests with Holm correction). (D) Daily sucrose consumption for the 3 archetypes (pairwise Wilcoxon tests with Holm correction). (E) Repartition of archetypes per experiment showed that they are not evenly represented in each group ($N = 32$, red dot indicated mean values, left) and built theoretical densities expected for each archetype based on a random draw from mean groups sizes (Bandwidth = 0.1, $n = 10,000$, right). Data can be found here https://zenodo.org/uploads/13374058.

(i.e., whether the sucrose is on the left or right). Despite some recurring patterns, there are considerable variations in these parameters between mice (Fig 2A, bottom).

To better describe this variability, we used archetypal analysis, an unsupervised approach for identifying behavioral clusters [38,45,46]. It depicts individual behavior as a continuum within an archetypal landscape defined by extreme strategies: the archetypes. The five-dimensional data set characterizing individual responses was used to identify 3 archetypal phenotypes. Individual data points are thus represented as linear combinations of extrema (vertex corresponding to archetypal strategies) of the data set, i.e., each mouse is represented by a triplet of α coefficients describing the archetypal composition and can be visualized with a ternary plot (Fig 2B, top). The 3 archetypes distinguish Trackers (Tr) who track the sucrose position (Fig 2B, top right, see mouse i as an example), from Explorers (Ex) who choose almost randomly between the left and right side on each trial (Fig 2B, middle right, see mouse j) and Non-Switchers (NS) who choose the same side throughout the majority of the sessions (Fig 2B, bottom right, see mouse k). Subsequent analysis highlights that these 3 profiles are distinguished not only by the choice parameters in the T-maze (used in their construction), but also by sucrose consumption and number of entries in the T-maze, reinforcing the definition of the profiles as personality-like categories. Trackers enter the T-maze frequently (i.e., high number of trials per day), whereas Non-Switchers rarely enter it (Fig 2C, left). In terms of choice, Trackers go most often to the sucrose side (Fig 2C, right) and consume more sucrose than the others (Fig 2D). Finally, the 3 profiles are distributed across the different experimental groups ($N = 32$) tested (mean = 8.8 mice per group, min = 5, max = 10) with an average proportion in a group of 37.4% for Trackers, 44.6% for Explorers, and 18.0% for Non-Switchers. The observed distribution of proportions within a group (Fig 2E, left) is consistent with a random sampling (Fig 2E, right) of a profile for each animal (with the corresponding probability) within group sizes similar to those obtained experimentally.

Reward-seeking strategy in isolation correlates with behavioral trait variation in the social compartment

Behavior in the T-maze is fundamentally different from behavior in the main environment. In the T-maze, animals are isolated from any direct influence from other animals and are left to make their own decisions. This is not the case for behavior in the main environment, where all behaviors are potentially subject to the consequences of social interactions. Because of these strong differences in context, we wondered whether the differences in strategy observed in the T-maze would also correspond to behavioral differences in the main environment, suggesting that mice strategies can serve as a marker of individual profiles across multiple levels of analysis.

The analysis of mouse behavior in the main environment is based on their detection by antennae located on the 3 transition tubes between the compartments. Compared to mice with other archetypally defined profiles, Trackers showed an increase in the average number of tube antenna detections per day (NbD, Fig 3A). They also have a reduced probability of transitioning from Nest to Food compartments (%$NtoF$, Fig 3B). A strong inverse correlation was observed between NbD and the %NtoF across all mice, regardless of their archetypal profile (Fig 3C). This suggests a more nuanced relationship between these variables than what can be captured by simple group statistics and reinforces the idea that mice can be individually defined by their behavioral repertoires, indicative of a profile for each mouse. Because the archetypal framework defines each individual as a linear combination of the 3 possible profiles, this analysis can be further refined by introducing the notion of distance from the archetype. The archetypal composition (i.e., given by α_k with k the archetype, Fig 3D) reflects this
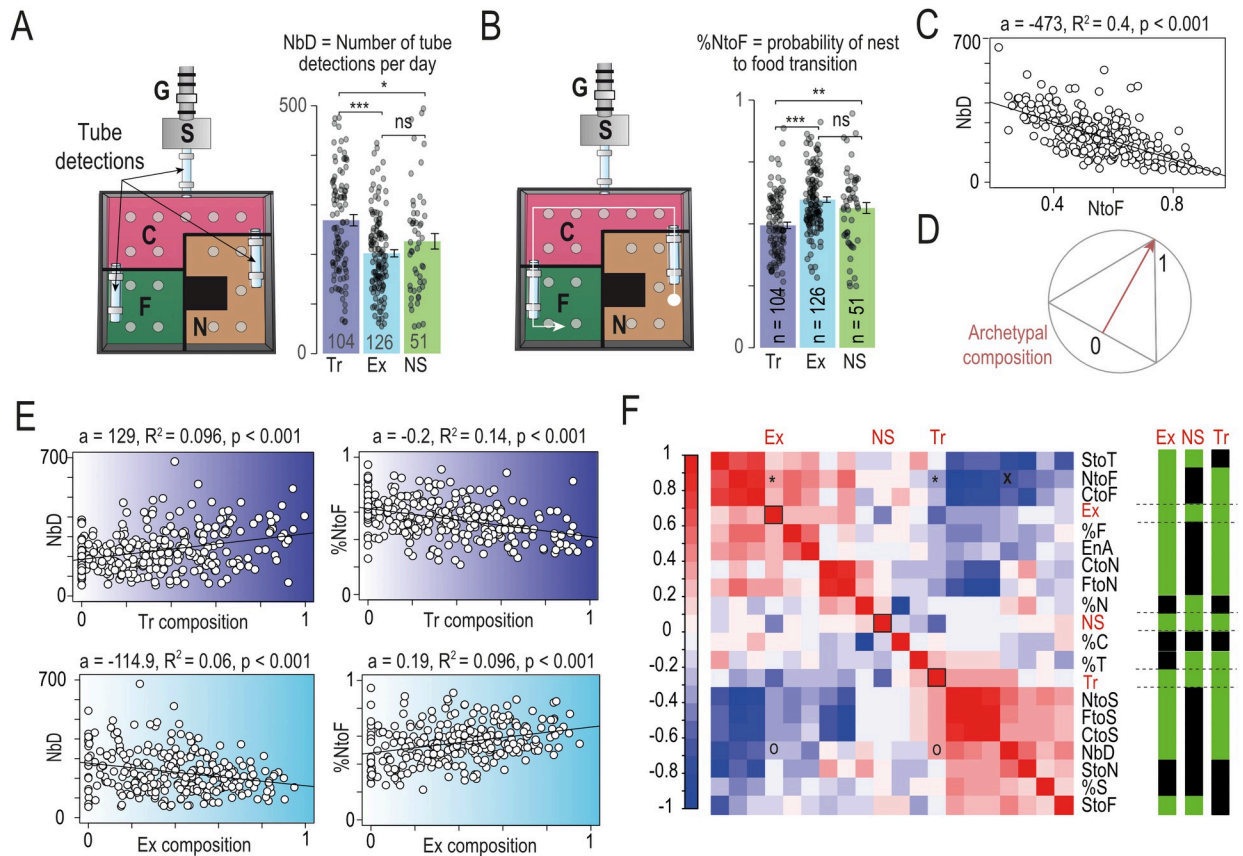
Fig 3. Archetypes defined by individual choices capture variation in the social cage behavior. (A) Activity in the main environment, estimated by the number of transitions between compartment (NbD), for the 3 archetypes (pairwise Wilcoxon tests with Holm correction, 3 points above 500 were not plotted). (B) Probability of nest to food transition (NtoF) for the 3 archetypes (pairwise Wilcoxon tests with Holm correction). Data can be found here https://zenodo.org/api/records/13374058/draft/files/Fig 3A-B.csv/content. (C) Correlation between NtoF and NbD. (D) Principle of archetypal composition measurement: the archetypal composition (i.e., given by α_k with k the archetype) would be equal to 1 if the mouse is exactly at the point of the archetype, and 0 if it is on the opposite side. (E) Correlation (linear regression, a indicating the slope estimate, R^2 the Adjusted R-squared and p the *p*-value) between Tracker (Tr) composition and pNtoF (left) and NbD (right), respectively (top), and between Explorer (Ex) composition and pNtoF (left) and NbD (right), respectively (bottom). (F) Left: Correlation matrix (Pearson correlation coefficient) of main environment variables and archetypal profile. Right: *p*-value for correlations. Green: $p < 0.05$, Black: $p > 0.05$. Variables: Activity Levels: Number of Detections (NbD), Entropy (EnA); Probability of Transitions: Stair to T-maze (StoT), Nest to Food (NtoF), Center to Food (CtoF), Center to Nest (CtoN), Food to Nest (FtoN), Nest to Stair (NtoS), Food to Stair (FtoS), Center to Stair (CtoS), Stair to Nest (StoN), Stair to Food (StoF); Occupancy: percent time in Food compartment (%F), percent time in Nest compartment (%N), percent time in Center compartment (%C), percent time in T-Maze compartment (%T), percent time in Stair compartment (%S); Archetypes: Explorer (Ex), Non-Switcher (NS), Tracker (Tr). * and ° indicates correlation between Tr and Ex composition with pNtoF and NbD shown in (E). X indicates correlation shown in C.

https://doi.org/10.1371/journal.pbio.3002850.g003

distance: its value is between 0 and 1, with 1 being if the mouse is exactly on the archetype, and 0 if it is on the opposite side of the archetypal space. We found that *NbD* increases across mice as their composition approaches the pure Tracker archetype, while their %*NtoF* decreases (Fig 3E, top). However, these 2 relationships are reversed for the Explorer archetype composition, such that *NbD* decreases and %*NtoF* increases as the composition of the mice approaches the pure Explorer archetype (Fig 3E, bottom). These correlations reflect both profile differences and environmental constraints (i.e., the structure of the settings) on behavioral expression.

We next systematically analyzed the linear correlation between an individual's archetypal composition and specific behaviors in the main environment (Fig 3F, right). Three categories of variables were used to describe activity levels (Fig 1C), compartment occupancy (Fig 1D), and transitions, respectively (Fig 1E). Robust correlations were found between the variables

describing these categories and the archetypal compositions, with the pattern of these correlations also discriminating between archetypal profiles (Fig 3F, left). Interestingly, Explorer and Tracker archetypes often exhibit correlations with the same behaviors; however, these correlations are inversely related. For example, Explorer composition was positively correlated with the transition from the central to the food or the nest compartment, and negatively correlated with the transition from the central to the stair compartment. In contrast, Tracker composition was positively correlated with the transition from the central compartment to the stairs, and negatively correlated with the transition between the central and nest or food compartments. This suggests that Explorer and Tracker could be construed as contrasting profiles within the primary environment. Non-Switchers display a profile that is markedly distinct from the other 2 profiles (Fig 3F, right). They are characterized by a preference for the nest compartment (S1A Fig). Comparing the archetypes reveals that Trackers are the least likely to go to the food compartment, either directly from the central compartment (S1B Fig) or by passing through it from another compartment (S1C Fig) where they spend less time than the other archetypes (S1A Fig). Explorers are the most likely to transition from the Stair to the T-maze, although the time spent in the stair (%S) is not different, suggesting they wait less in the Stair to enter the T-Maze (S1A and S1B Fig). Non-Switchers, in particular, showed a propensity to transition from the Stair to the Nest or Food compartments (via the Central compartment), indicating that these mice are the least likely to re-enter the Stair to engage in the task (S1D Fig). Archetypal groups did not differ in their entropy, despite differences in the number of tube detections, suggesting that while Trackers move more between compartments, all mice share roughly the same territory within Souris-City (S1D Fig).

Overall, these analyses suggest that individual mouse profiles extend beyond variations solely within reward seeking strategies in the T-maze to also encompass differences in activity within the main compartment. These relationships between individualistic strategy development and trait expression can be considered as a foundation of mice "personalities," which emerge as adaptive responses to their complex environment.

Distinct reward-seeking profiles are defined by individual differences in learning rate and sensitivity to value

Because decision-making strategy is a good marker for individual profiles of mice in Souris-City, we next aimed to decompose the latent variables that individual mice use to define their strategy. The decision-making process of an individual mouse in the T-maze can be seen as a series of binary choices between going left or right in an unpredictable environment. It is assumed that the animal learns the value assigned to each option (left or right) and that it adapts to the change (every 3 to 4 days) in the position of the rewards (sucrose or water). In this context, we fitted each individual's choice data with a standard reinforcement learning model [47], which uses the sequence of choices to estimate the expected value of each option for each trial. The reward value for the water option was set to 1, and the sucrose option was set to 3, for a ΔV of 2. The value of the chosen option (V_L or V_R for left and right side, respectively) was updated after each trial using a reward prediction error rule (see methods) and a learning rate α that sets how rapidly the estimate of expected value is updated on each trial. Given expected values for both options, the probability of choosing the right option $P_R(t)$ is computed using a SoftMax rule with 2 parameters: the inverse temperature parameter β which represents the sensitivity to the difference of values and a choice perseveration parameter χ that captures short-term tendencies (previous choice) to perseverate or alternate (when positive or negative, respectively; Fig 4A, left). This propensity to alternate is independent of the reward history [48], and thus does not depend on ΔV. We fitted the choice data of each mouse
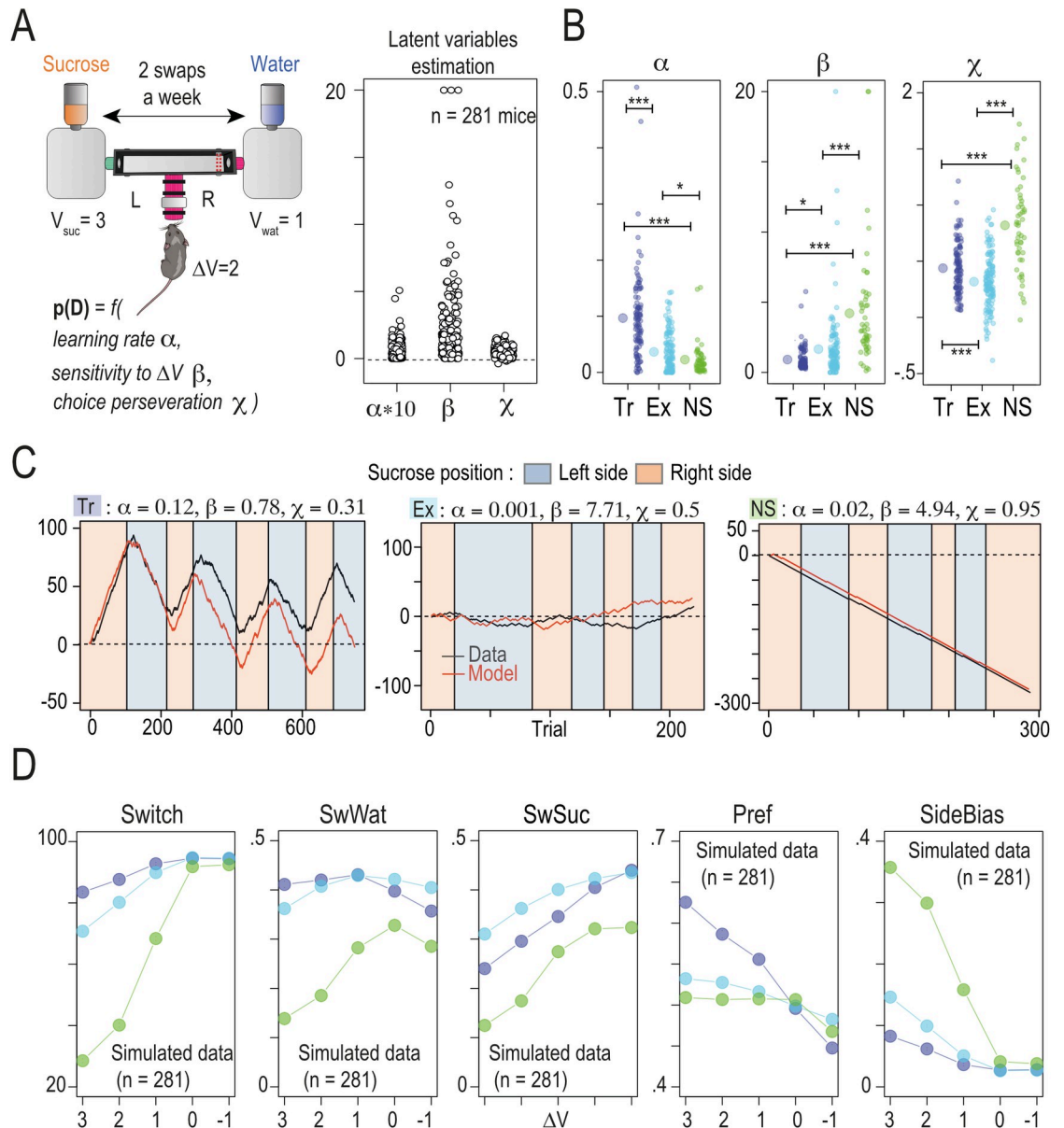
Fig 4. Computational modeling suggests that decision and learning parameters differ between the 3 archetypes. (A) Left: Principle of the reinforcement learning and SoftMax model, with 3 Latent variables α (the learning rate), β (inverse temperature or sensitivity to the difference of values ΔV), and χ (the choice perseveration). The theoretical value of water and sucrose are set to 3 and 1, respectively. Right: Estimated values of α, β, and χ for $n = 281$ mice. **(B)** Latent variables according to the Tr, Ex, and NS archetype (left symbol: mean ± SEM, Wilcoxon tests with Holm correction, right: individual value per mice). Data can be found here https://zenodo.org/api/records/13374058/draft/files/Fig4A-B.csv/content. **(C)** The model recapitulates the profiles drawn from experimental data (same example as in Fig 2B) when fitted with individual triplets values for the latent variables of each individual of a specific archetype. **(D)** Comparison of the mean of 5 variables (*Switch*, *SwWat*, *SwSuc*, *Pref*, *SideBias*) for Tr, Ex, and NS archetype obtained for 5 differences in the value (ΔV, one side as a value of 1) associated with the choice (6 sessions of 50 choices, simulated with fitted values of α, β, and χ, $n = 281$).

https://doi.org/10.1371/journal.pbio.3002850.g004

with this model and obtained triplet of latent variable values (α, β, and χ; Fig 4A, right) for each individual (see Methods). The 3 archetypes extracted from the sequence of choice corresponded to different combinations of α, β, and χ (Fig 4B). These parameters also correlate with the number of trials in the T-maze (S2A Fig, α: $p = 0.002$; $R^2 = 0.03$; β: $p = 7e^{-8}$, $R^2 = 0.1$;

χ: p = 2e^{-5}, R^2 = 0.06), indicating that these latent variables capture information that is not directly linked to the decision process. Finally, when we use this model to simulate data under the constraints of experimental trial sequences (same number of trial) and rewards (water/sucrose, right or left), we can differentiate the same 3 types of profiles that we find in the experimental data (Fig 4C). One question, however, is whether the estimated latent variables (Fig 4A) or the dynamics of the choices (Fig 4C) simply reflect a difference in the number of trials, as individuals who entered the T-Maze the least were indeed less likely to find the sucrose. To test this hypothesis and to decorrelate our results from a possible difference due to a variation in the number of trials, we modeled the behavioral profiles (*n* = 281 mice) from the latent variables (α, β, and χ, 1 triplet per mice) with 6 alternating sessions (sucrose/water left or right) of 50 trials each. Our model with 3 latent variables explained the phenotypic variables *(Switch*, *SwWat*, *SwSuc*, *Pref*, and *Side Bias)* very well, regardless of the number of trials (S2B Fig).

Having demonstrated the validity of our model, we next questioned the relative importance of each latent variable in explaining the observed results by designing an attribution study in which each of the latent variables (α, β, or χ) is manipulated independently from the other. We then simulated the data and compared the results obtained using (i) the latent variable values estimated for each mouse associated with each profile; (ii) by randomly picking latent variable triplets from the set of estimated values; and (iii) by using 2 estimated values for each individual and randomly picking the third from the set of possible values obtained (S2C Fig). This analysis reveals that the χ parameter plays a minimal role in the differentiation of the profiles. In other words, the choice perseveration parameter does not contribute significantly to the observed variations within the profiles. Finally, when we simulate data with randomized parameters (α, β, and χ) while keeping the experimental numbers of trials from each individual's experimental data, we do not replicate the difference between profiles. This simulation supports the conclusion that the behavioral profile cannot be attributed to variations in the number of trials (S2C Fig, gray points). Overall, the Tracker archetype is associated with a high α value and low β, consistent with individuals who are able to quickly update their value representation and thus favor sucrose tracking. The Explorer archetype is characterized by an intermediate α and β, and thus an important level of switching from one trial to the other. In contrast, the Non-Switchers are associated with low α and high β, a combination that favors profiles in which the animals remain mainly on one side, in particular the side with the highest initial value representation (this representation is updated slowly due to a low α). Indeed, the majority of Non-Switchers showed a bias for the side on which they first encountered the sucrose (33/51) or the side where they found sucrose for the majority of their first choices and (2/51) (S2D Fig). The other Non-Switcher mice (16/51) chose the side corresponding to their initial preference during the WW session.

Reward-seeking strategy defines adaptability to changes in reward value and predicts nicotine choice

We next asked if an individual's profile, defined as a combination of their latent variables, could predict how they would adapt to other choice situations. In a binary choice, such as in the T-maze, a major external variable is how the value between the 2 options differs. We thus simulated the theoretical response of the different profiles, namely Tracker, Explorer, and Non-Switcher, to changes in reward values difference (ΔV) in the T-maze. One of the values is fixed at 1 (corresponding to the value given to the reference solution, e.g., water), the other value varies between 0 and 4 to give a scale of ΔV between −1 (less valued than the reference) and 3 (more valued than the reference). Variation in the 5 choice variables revealed different adaptations to ΔV depending on the profile (Fig 4D), with the simulated data at ΔV = 2
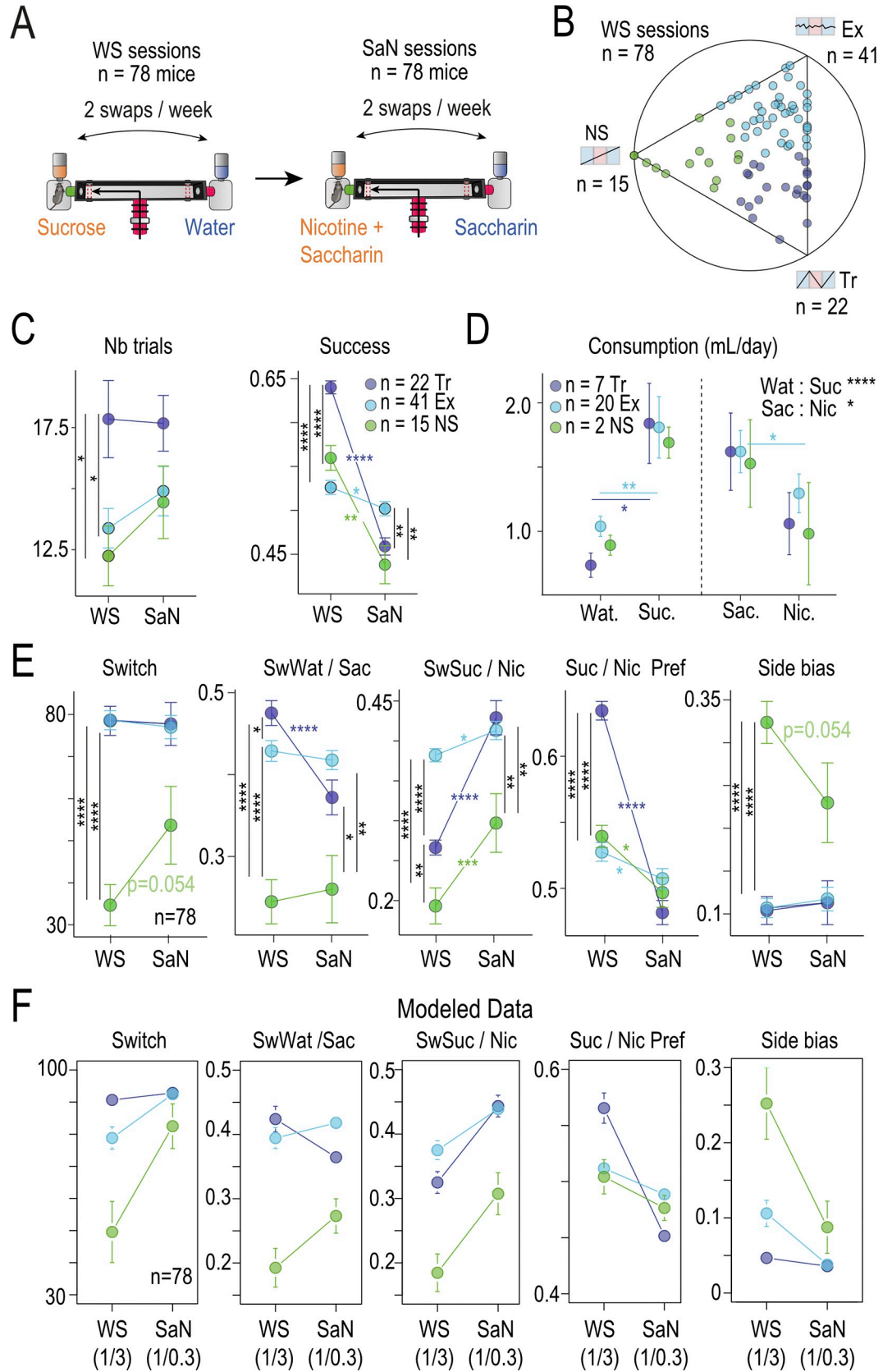
recapitulating the behavioral data for the choice between Water and Sucrose. The Explorer-archetype is characterized by little adaptation of their choice with changes in ΔV, whereas Tracker and Non-Switcher archetypes show strong adaptation. Trackers show a clear side preference for the higher value, and this preference increases as ΔV increases. Finally, the most surprising result comes from the Non-Switcher profile. Their side bias is clearly not independent of ΔV, but becomes more important as the value difference increases: the higher the ΔV, the more the mice stick to one side of the T-maze. This simulation thus suggests that our 3 profiles adapt completely differently to changes in reward in the T-maze.

We tested this idea by conducting an experiment in which the mice were exposed to 2 consecutive sessions with different test solutions. This experiment allowed us to modulate ΔV and test whether the animals behaved as predicted by the model, i.e., adapting their choice in response to the new outcome values. Hence, a subgroup ($n = 74$) of the 281 mice was subjected to a period (SaN) of choice between nicotine (100 μg/ml) plus 2% saccharin (Nic) versus 2% saccharin alone (Sac) in the T-maze, following the prior water versus sucrose period (WS) (Fig 5A). The mouse behavior during the WS session showed a typical distribution of mice among the 3 profiles in the archetypal space (Fig 5B). During the SaN period, there was a global decrease in the number of successful choices (with nicotine considered the successful choice), but no significant change in the number of trials per day (Fig 5C). Additionally, the consumption pattern changed, as mice consumed more sucrose than water in the WS period, whereas they consumed as much saccharin as nicotine in the SaN period (Fig 5D). Together, these results suggest that the ΔV between nicotine + saccharin and saccharin alone is smaller than the ΔV between water and sucrose.

Next, we examined changes in the 5 variables (Switch, SwWat, SwSuc, Pref, and Side Bias) that describe the choice behavior in the T-maze across the 2 periods (Fig 5E). Consistent with the simulation predictions, there were no modifications in these 5 variables for the Explorer between WS and SaN periods, suggesting a minimal adaptation to the change in ΔV. In contrast, significant adaptations were observed in the Tracker and Non-Switcher profiles. The Trackers displayed a decrease in preference (Suc/Nic Pref) and switch behavior after choosing the saccharin side (swWat/Sac), but an increase in switch behavior after choosing the nicotine side (swSuc/Nic). On the other hand, the Non-Switchers primarily showed an increase in switch behavior after receiving the reward (swSuc/Nic). In the SaN period, Trackers and Explorers were similar for all variables, and different from the Non-Switchers. Similar results were obtained by simulating the response of the different profiles—Tracker, Explorer, and Non-Switcher—to changes in reward values in the T-maze (Fig 5F). For this comparison, the values for the reference solutions (water or saccharin) were set at 1, the value for sucrose was maintained at 3 (Fig 4A), and the value for nicotine + saccharin was estimated to be 0.3. This demonstrates that the model and the latent variables effectively capture the information needed to model the behavior of mice under different reward values, depending on their profile. In addition, the model accurately predicts the behavioral response to the choice between nicotine + saccharin and saccharin alone, a choice with a smaller ΔV in comparison to water versus sucrose. Our behavioral and modeling results support the notion of individual profiles defined by latent variables which constrain the expression of behavior depending on the context and the value of the rewards.

Neural correlates of adaptability to the environment emerge after nicotine challenge
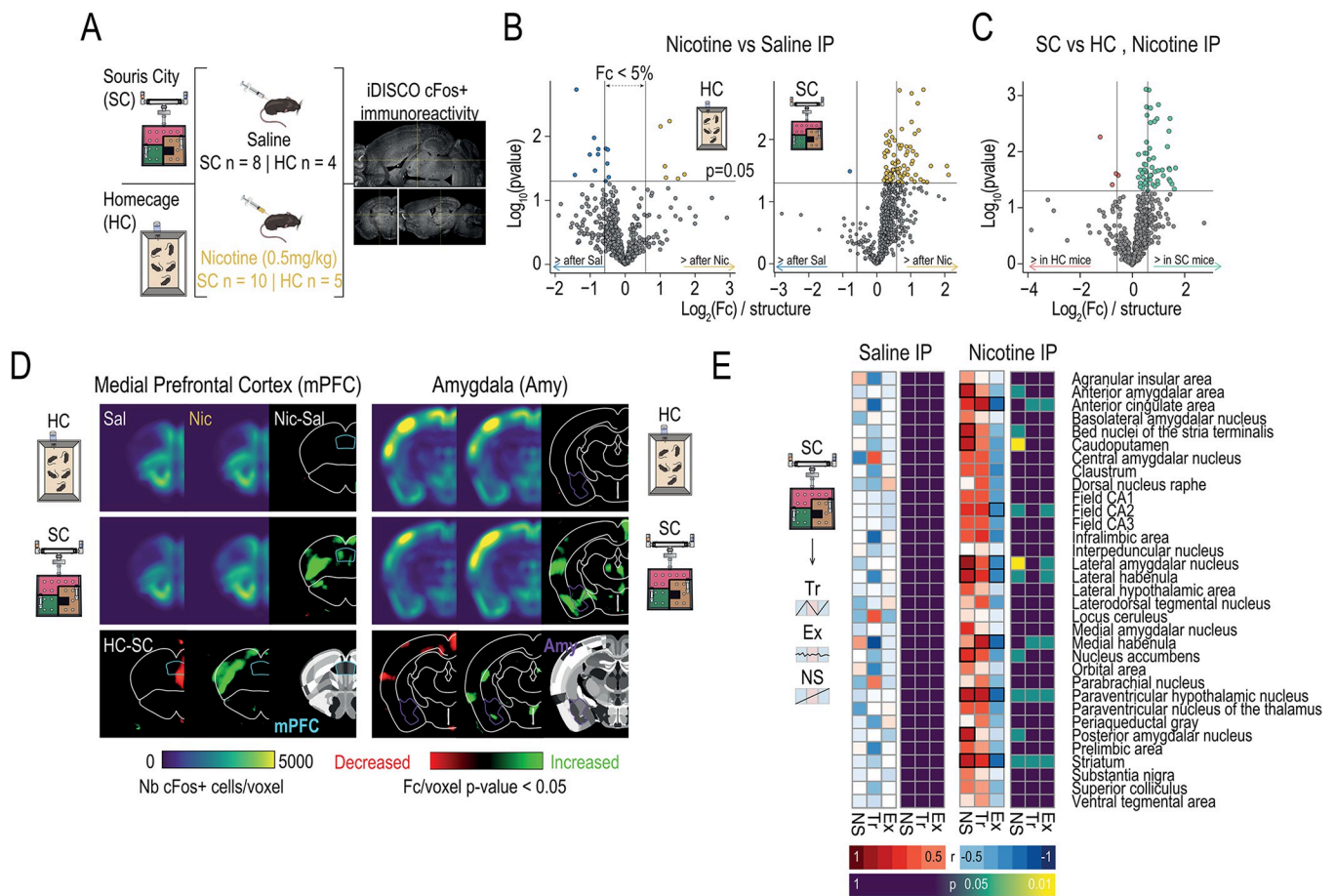
To determine how adaptation to environmental conditions influence the neural response to nicotine, we compared brain-wide cellular activity after an injection of nicotine or saline

Fig 6. Differential response to nicotine as a function of the environment and decision-making strategy. (A) Brain-wide cFos expression mapping after saline or nicotine injection in mice living in standard home cages (HC) or Souris-City (SC) revealed by iDISCO brain clearing and Clearmap. **(B)** Mice in HC conditions do not show significant differences in cellular activity between saline and nicotine injections, while mice in SC show a shift toward increased cFos expression (greater fold change of the number of cFos+ cells per region) following a nicotine injection when compared to a saline one. **(C)** Comparison between nicotine-induced cFos expression in SC and HC mice reveals that SC mice show greater numbers of cFos-positive cells per region in response to nicotine than mice raised under standard conditions. **(D)** Grouped heatmaps show average density of cFos-positive cells in the PFC (left) and the amygdala (right). *P*-value maps highlight areas where significant between-groups differences can be appreciated. **(E)** Correlations between cFos expression and distance to the archetype in saline and nicotine-injected SC animals. Left: minimal differences in cFos expression are observed between mouse profiles in SC in response to a saline injection. Right: patterns of expression across brain regions associated with cognitive and reward functions that become apparent after challenging the different mouse profiles with nicotine.

https://doi.org/10.1371/journal.pbio.3002850.g006

between mice living in Souris-City (at the end of SW session) and those living in standard home-cage housing (Fig 6A). Cellular activity in response to a challenge injection of saline or nicotine, measured as the numbers of cells expressing the immediate-early gene cFos, was compared between home-cage and Souris-City mice using the iDISCO+/ClearMap pipeline

Fig 6. Differential response to nicotine as a function of the environment and decision-making strategy. (A) Brain-wide cFos expression mapping after saline or nicotine injection in mice living in standard home cages (HC) or Souris-City (SC) revealed by iDISCO brain clearing and Clearmap. **(B)** Mice in HC conditions do not show significant differences in cellular activity between saline and nicotine injections, while mice in SC show a shift toward increased cFos expression (greater fold change of the number of cFos+ cells per region) following a nicotine injection when compared to a saline one. **(C)** Comparison between nicotine-induced cFos expression in SC and HC mice reveals that SC mice show greater numbers of cFos-positive cells per region in response to nicotine than mice raised under standard conditions. **(D)** Grouped heatmaps show average density of cFos-positive cells in the PFC (left) and the amygdala (right). *P*-value maps highlight areas where significant between-groups differences can be appreciated. **(E)** Correlations between cFos expression and distance to the archetype in saline and nicotine-injected SC animals. Left: minimal differences in cFos expression are observed between mouse profiles in SC in response to a saline injection. Right: patterns of expression across brain regions associated with cognitive and reward functions that become apparent after challenging the different mouse profiles with nicotine.

https://doi.org/10.1371/journal.pbio.3002850.g006

[49]. Mice living in Souris-City showed a greater differential activity across the brain in response to an acute nicotine challenge (Nicotine versus Saline injection, Fig 6B, right) than mice living under standard HC conditions (Fig 6B, left). Furthermore, mice in SC had overall greater brain-wide activity in response to an acute injection of nicotine than mice in HC (Nicotine HC versus Nicotine SC, Fig 6C), including significant increases in cFos positive cells in regions associated with addiction, such as the medial prefrontal cortex, as well as in parts of the amygdala associated with anxiety and anxiety-like behavior. Indeed, voxel-by-voxel comparisons in these regions identify significant increases in activity only in the SC mice that received a nicotine injection (Fig 6D), suggesting that the adaptability required simply by living in a complex micro-society environment reorganizes brain-wide responsivity to nicotine. We next asked whether the distinct reward seeking profiles identified in SC, which are notably associated with distinct adaptations in the face of changing reward values, show differential activation of brain regions in response to nicotine injection. We correlated each mouse's archetypal composition with their cFos-positive cell counts in response to saline or nicotine injection in 33 regions known to show alterations in cFos expression in response to nicotine [50,51]. The number of cFos-positive cells did not correlate with archetypal composition following a saline injection in any of the brain regions studied (Fig 6E, left). Following a nicotine injection, however, marked patterns of correlations are evident (Fig 6E, right): mice that show adaptations in response to ΔV in the T-maze, namely the Tracker and the Non-Switcher archetypes, showed strong positive correlations across one third of the predefined regions, whereas the Explorer mice showed largely negative correlations. Increases in cellular reactivity to this nicotine challenge may thus be linked to behavioral and choice adaptability in the face of changing reward values.

We observed altered reactivity to nicotine across many brain regions, notably including dopamine receptive regions (e.g., the striatum) and regions that regulate dopamine neuron firing (e.g., the lateral habenula). Thus, we next asked if adaptation to the SC environment would also lead to alterations in VTA DA neuron activity. We first used in vivo juxtacellular recording to assess the spontaneous activity of VTA DA neurons between mice immediately upon their exit from SC and compared this with HC mice. Because the exposure to sucrose in the SC environment could, in and of itself, alter DA activity, 2 groups of HC mice were studied: one with access only to water (HC/Wat) and one with access to a 5% sucrose drinking solution (HC/Suc) (Fig 7A). Both the firing rate and the bursting activity (%SWB) of VTA DA cells were significantly higher in mice with access to sucrose as compared to water in HC condition (Fig 7B). In Souris-City, VTA DA cells showed intermediate firing rate and an overall reduced bursting rate compared to the 2 HC conditions. These results confirm that while sucrose exposure alters DA neuron activity, it is not sufficient to explain the differences we find in SC. Thus, both sucrose exposure and the environment interact to modulate VTA DA cells activity [5].

To dissect whether the differences that we observed in spontaneous VTA DA neuron activity in SC mice are related to mouse profiles, we categorized the SC mice according to their archetypes (Fig 7C, left, n = 85 mice). Comparing basal DA neuron activity between the archetype groups revealed a significant difference in firing rate between the Explorers and Non-Switchers (Fig 7C, right). Averaging dopaminergic activity per mouse revealed a correlation between the proximity to the archetype and the firing rate for Explorers (Fig 5D, right, p = 0.028) but not for Trackers (Fig 7D, left, p = 0.08) or Non-Switchers (p = 0.8). We then measured nicotine-evoked responses in anesthetized animals to investigate whether the environmental condition impacts the sensitivity of DA neurons to nicotine (Fig 7E). VTA neurons are not a uniform population and we have shown that nicotine concomitantly activates and inhibits 2 distinct subpopulations of DA neurons [52,53]. Therefore, when recording the
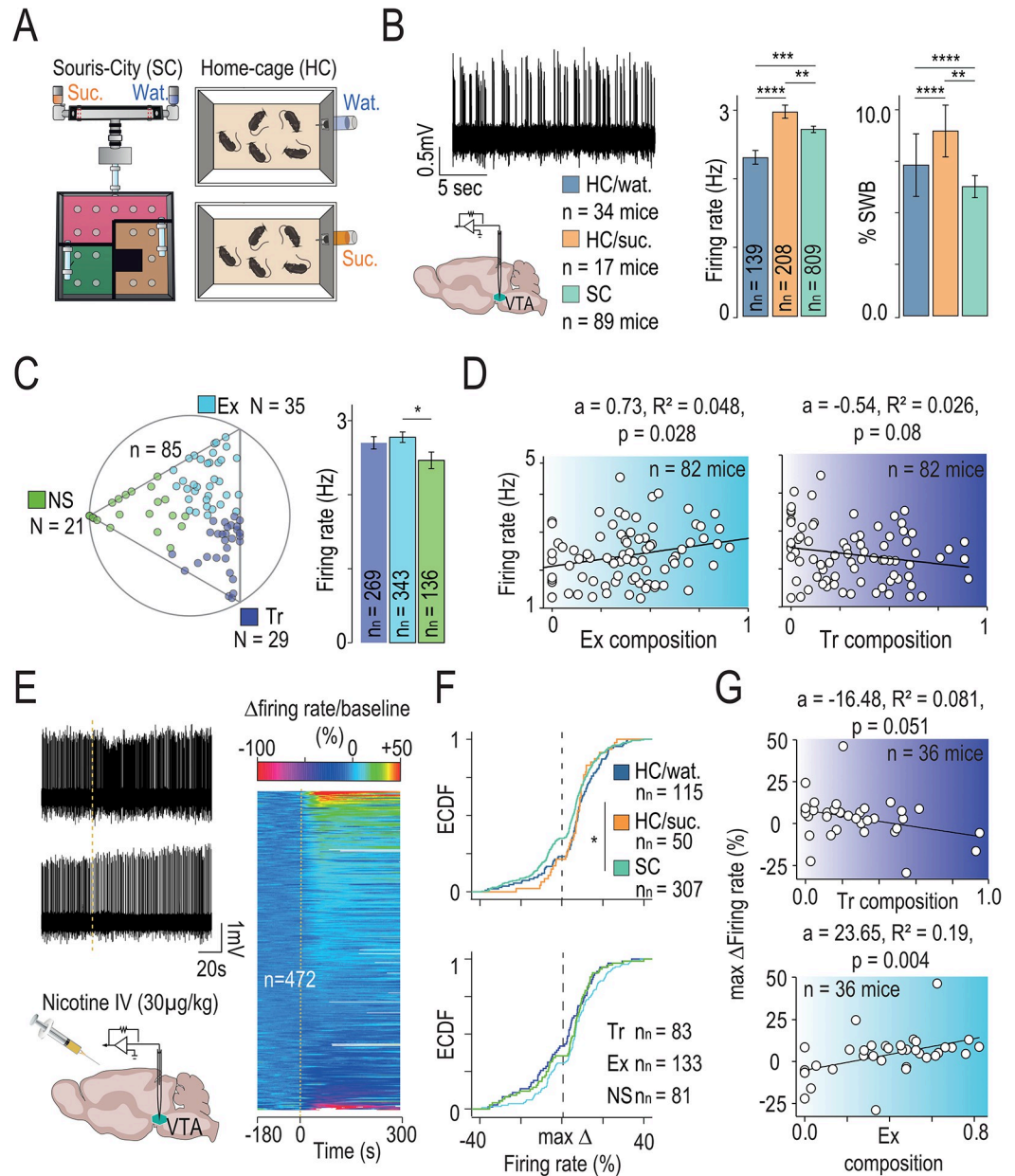
Fig 7. Dopamine neuron firing is modulated by both the environment and mouse profile. (A) Spontaneous activity of VTA dopaminergic (DA) neurons recorded in mice living in standard home cage (HC) with access either to water (Wat) or to a 5% sucrose drinking solution (Suc) or in Souris-City (SC). **(B)** Mean firing rate and percentage of spike within burst (% SWB) are different in the 3 groups (Kruskal–Wallis (df = 2, p = 0.017) and post hoc Wilcoxon tests with Holm correction, *$p < 0.05$, n indicated number of mice, nn indicated number of neurons). Data can be found here https://zenodo.org/api/records/13374058/draft/files/Fig 7B.csv/content. **(C)** Left: Position in the ternary plot of the n = 85 mice used in this analysis. Right: Firing rate in Hz according to the archetype (Wilcoxon tests with Holm correction, n = 748 neurons). **(D)** Correlation (linear regression, a indicated the slope estimate, R^2 the Adjusted R-squared and p the p-value) between Explorer (Ex, left) or Tracker (Tr, right) composition and median firing rate per mice (n = 82 mice, with a minimum of 3 cells per mice). **(E)** Left: Intravenous (i.v.) injections of nicotine (Nic; 30 μg/kg) induce activation (upper panel) or inhibition (lower panel) of distinct VTA DA neurons in anesthetized mice (representative recordings). Right: Responses of VTA DA neurons after nicotine injection. Responses are rank-ordered based on the response to nicotine, from the most excited to the most inhibited (top to bottom of the graph). Color scale indicates variation in firing rate amplitude. **(F)** Empirical cumulative distribution of the response to nicotine (variation in firing rate). (Top) Neurons recorded in mice living in Souris-city, in home cage (HC) with water (HC/Wat) or with sucrose drinking solution (HC/Suc) (Kruskal–Wallis (df = 2, p = 0.011) and post hoc Wilcoxon tests with Holm correction, *$p < 0.05$). (Bottom) Neurons recorded in SC mice according to their Tr, Ex, and NS respective profiles (Kruskal–Wallis (df = 2, p = 0.059)). **(G)** Correlation between Tracker (Tr, top) or Explorer (Ex, bottom) composition and median response in firing rate per mice (n = 36 mice, with a minimum of 5 cells per mice).

https://doi.org/10.1371/journal.pbio.3002850.g007

response of a population of DA neurons to nicotine, they can be organized from the most excited to the most inhibited (Fig 7E, right). Comparison of the distributions according to the environment reveals differences (Fig 7F, top, HC/suc versus SC, $p = 0.013$) while comparison of the distributions according to the profiles observed in SC (Fig 7F, bottom) did not highlight reliable differences ($p = 0.059$). On the other hand, we observed clear correlations between the proximity to the Tracker and Explorer archetypes and the median response per animal (Fig 7G). The maximum change in firing rate after nicotine injection increased as mice approach the pure Explorer archetype, while it decreases as mice approach the Tracker archetype. This opposition in dopamine neuron response to nicotine between the 2 profiles mirrors the contrast seen in their behavioral patterns, latent variables, and adaptability to changing outcome values.

Together, these data indicate the existence of correlations between sucrose-seeking patterns in a choice task and the response to nicotine, suggesting that adaptations in dopaminergic circuit function emerge between mice profile identified by their decision-making strategies.

Conclusions

In this study, we found that a complex social environment reveals interindividual differences in mouse reward-seeking strategy, even when tested isolated from their peers. In a previous study [5], we showed that these differences are the consequences of individual adaptation to the environment. Here, we show that these differences are further linked to variations in behavioral traits (or "personality"), in the activity of the dopaminergic system, and in the response to nicotine. By using a reinforcement learning (RL) model trained on a specific choice situation (water versus sucrose), we were able to accurately predict the animals' behavior in a different situation involving a choice between saccharin alone and saccharin with nicotine. These results suggest that in a complex social environment (i) animals adopt distinct foraging strategies; (ii) these strategies reflect individual traits and the state of neural circuits; and (iii) an individual's strategy can be indicative of their response to addictive substances. Overall, the study highlights how harnessing interindividual variability in behavior and its underlying mechanisms, particularly in the context of addiction research, can unravel more complex and nuanced relationships between neural circuits and behavior than would be possible by assuming that all mice should respond uniformly to a task. The use of large naturalistic environments with automated data capture provides a valuable tool for studying individual variations and their implications for the development and maintenance of individual profiles and susceptibility to substances of abuse like nicotine.

There is ongoing debate regarding the emergence of interindividual variation and the concept of "personality." Our experiments demonstrate that when animals are placed in controlled, yet naturalistic environments, distinct profiles, marked by clusters of behavioral traits, emerge and remain stable over extended periods, which can be considered the definition of "personality." Being able to test animals in isolation in a simple choice test eliminates direct social influences and mitigates issues related to multicollinearity and co-dependence in the main environment. This approach also reveals the complexity of the underlying mechanisms. The broad concept of cerebral plasticity and the embedding of an individual in an environment allow for the consideration of each individual's singularity. This singularity is manifested through differences in neural connections and activities, but that alone is insufficient to explain interindividual variability and the emergence of stable differences. Connections and activities themselves are modified by an individual's history and by the environment in which they live [54]. No 2 animals can live in exactly the same environment, as how each individual engages with their physical surroundings and social milieu will be different as a function of

their bodily constraints and personality traits (e.g., their level of sociability). Thus, even when animals live in the same physical space they necessarily adapt differently. Studies involving grouped animals have demonstrated this adaptability, showing that initial diversity reemerges when animals with similar profiles are grouped together [5]. The asymmetry of the environment, which includes social relations and competition for resources, facilitates the development of individuality, with both shared and non-shared components within each individual's perceived environment [3,55]. When an animal is exposed to a test, isolated from the others, the differences in strategies that can be seen in the test reflect the differences that exist in the main environment and are the consequences of each individual's adaptations to both that environment and its co-living congeners. In our study, this is reflected in differences in dopaminergic activity, responses to nicotine, and strategies employed in the T-maze.

Differences in the T-maze can be captured by reinforcement learning models. Variances observed in a specific choice context (water-sucrose) can be explained by discrepancies in learning rates and exploration parameters. These models accurately predict how responses evolve when the difference in value between proposed rewards is changed. These results confirm the validity of these computational approaches to account for behavior and the use of latent variables to describe such complex phenomena. Notably, the behavior of non-switchers animals becomes particularly intriguing within this context. While an initial judgment based on their side bias could conclude that these mice are insensitive to differences in value (i.e., low β), our modeling findings indicate that these animals in fact have a *high* exploitation level (high β), albeit paired with a very low learning rate, meaning that they update their representations slowly. When looking closer at their behavior, we indeed find that their bias is for the side where they encounter sucrose early on. This gradual and slow adaptation of value, combined with a strong bias toward the highest value and an environment characterized by rapid position changes of significant rewards, allows for the emergence of this seemingly "maladaptive" behavior. In a previous study, we were able to demonstrate that modifying the social environment, i.e., regrouping together non-switching animals, resulted in a fast re-adaptation of both the strategy and the dopamine firing pattern, suggesting an important impact of adaptation to the local environment [5,10]. If all latent variable values are a consequence of adaptation to the environment (both fixed and social), the remaining question pertains to the constraint that an individual must adapt in order to reduce its learning rate.

Finally, the differentiation of profiles observed in our study is closely linked to the unique patterns of spontaneous activity and response of dopaminergic neurons to nicotine. To fully understand the complex relationship between behavior and neural network activity, and to gain insight into drug susceptibility, it is imperative to systematically categorize individual differences. While it may be difficult to identify a single circuit responsible for behavior using current approaches, we can propose that the dopaminergic system, among others, occupies a central position at the intersection of several factors. On the one hand, the activity of the dopaminergic system is significantly influenced by an individual's personal history, social interactions, and cumulative experiences [5,10]. These factors shape the functional state of the dopaminergic system and ultimately influence its involvement in various behavioral processes. On the other hand, the dopaminergic system itself plays a central role in defining and regulating specific parameters related to decision making and behavioral expression [26,27,56,57]. It acts as a modulator, influencing the salience and motivational value assigned to stimuli and guiding the selection of appropriate actions in response to environmental cues. This central position of the dopaminergic system, shared by numerous brain regions, allows us to conceptualize a neural basis for the notion of individuality [10]. Thus, in this sense, our results suggest that a dynamic feedback loop exists between environmental condition and the dopaminergic system which continually defines animal traits and adaptability to future challenges.

By recognizing the complex interdependencies between neural activity, behavior, and environmental influences, we can gain a deeper understanding of the multifaceted nature of individual differences. This understanding is critical not only for unraveling the mechanisms underlying behavior, but also for elucidating the factors that contribute to susceptibility to drugs and addictive substances. Ultimately, a comprehensive exploration of these interrelated factors could allow us to develop more targeted and personalized approaches to addiction research and behavioral intervention.

Materials and methods

Materials availability

This study did not generate new unique reagents.

Experimental model. Experiments were performed on adult C57Bl/6Rj Wild-Type (Janvier Labs, France) mice. Male mice, from 8 to 10 weeks old at the beginning of the experiment, weighing 25 to 35 grams, were used for all the experiments. They were kept in an animal facility where temperature (20 ± 2°C) and humidity were automatically monitored and a circadian light cycle of 12/12-h light-dark cycle was maintained. All experiments were performed in accordance with the recommendations for animal experiments issued by the European Commission directives 219/1990, 220/1990, and 2010/63, and approved by Ethic Committee (APAFIS#25905–2020060516523945 v4/APAFIS#11061–2015072714306495 v6). All mice were implanted under anesthesia (isoflurane 3%–Iso-Vet, Piramal, United Kingdom), with an RFID chip subcutaneously inserted in the back.

Methods details

Souris City setup

Setup. Souris City combines a large environment (the social cage 1*1 m) where groups of male mice live for extended periods of time in semi-natural conditions and a test-zone where mice have a controlled access to specific areas for drinking. Souris City was house-designed and built by TSE Systems (Germany). Mice were tagged with RFID chips, allowing automatic detection and controlled access to the different areas. Animals were living under a 12h/12h dark-light cycle (lights on at 7 AM) and had access to food ad libitum. The social cage is divided into 4 sub-compartments. These different sub-compartments are equipped with RFID antennae on the floor and are connected through tubes that are also equipped with antennae. Therefore, each transition from one sub-compartment to another was associated with a detection of the animal by the 2 antennae of the transition tube [5].

The social cage is connected to the test zone by a gate, which is a key element of the setup. The gate (TSE Systems, Germany) is composed of 3 doors with independent automatic control. It allows for the selection of animals and grants control over their access to the test zone. In the test zone, mice are isolated from their peers and conduct the test on their own, without any intervention from the experimenter. The test consists in a T-maze choice task [58]. Since the T-maze was the only source of water, animals were motivated to perform the test. The T-maze gives access to 2 home-cages, one on each side (left and right), with a drinking bottle in each. The bottles contained either water, sucrose, saccharin, or nicotine. The system was configured in such a way that animals performed a dynamic foraging task. The reward value of the bottle content is changed every 3 to 4 days to evaluate whether mice were able to track the highest reward. Automating the task in this manner minimizes the need for human involvement, thereby mitigating limitations such as cost and time constraints associated with human assessment. Moreover, it eliminates the potential risks of inducing stress or disturbing the

natural cycle of the animals [59–62]. Simple rules were used to automatize the test. When a mouse accesses one liquid bottle, an infra red-light beam is interrupted in that particular arm, resulting in the closing of the access to the bottle on the opposite side. A Plexiglas cylinder descends, preventing access to the bottle. To initiate a new trial, mice must exit the T-maze, which triggers the reopening of the feeders. For the analysis in T-maze, throughout the paper, only mice accessing the T-maze more than 5 times per day are included in the analyses (i.e., 281/295). The only exception is in Fig 7B for the analysis of dopamine neuron activity after exposure to SC, where all mice are considered (in this group, 4 out of 89 mice made no more than 5 trials per day).

In vivo juxtacellular recordings of VTA DA neurons. Mice were deeply anaesthetized with chloral hydrate (8%), 400 mg/kg IP, supplemented as required to maintain optimal anesthesia throughout the experiment. The scalp was opened and a hole was drilled in the skull above the location of the VTA. Extracellular recording electrodes were constructed from 1.5 mm O.D./1.17 mm I.D. borosilicate glass tubings (Harvard Apparatus) using a vertical electrode puller (Narishige). Under microscopic control, the tip was broken to obtain a diameter of approximately 1 μm. The electrodes were filled with a 0.5% NaCl solution yielding impedances of 6 to 9 MΩ. Electrical signals were amplified by a high-impedance amplifier (Axon Instruments) and monitored through an audio monitor (A.M. Systems). The signal was digitized, sampled at 25 kHz, and recorded using Spike2 software (Cambridge Electronic Design) for later analysis. The electrophysiological activity was sampled in the central region of the VTA (coordinates from bregma: 3.1 to 4 mm AP, 0.3 to 0.7 mm ML, and 4 to 4.8 mm DV from the brain surface). Individual electrode tracks were separated from one another by at least 0.1 mm in the horizontal plane. Spontaneously active DA neurons were identified based on previously established electrophysiological criteria [29,63] and were not labeled after recording. Intravenous administration of saline (H_2O with 0.9% NaCl) or nicotine at a dose of 30 μg/kg (4.16 mg/kg, free base) was carried out through a catheter (30G needle connected to polyethylene tubing PE10) connected to a Hamilton syringe, into the saphenous vein of the animal.

Solution in T-maze experiment. In the T-maze, mice were presented with (i) 2 bottles of water; (ii) 1 bottle of water and 1 bottle of sucrose (5%, Sigma Aldrich); (iii) 1 bottle of saccharine solution (2%, Sigma Aldrich) and 1 bottle of nicotine (100 μg/ml free base, Sigma Aldrich) plus saccharine (2%) solution diluted in water (adjusted to pH ~7.2 with NaOH).

Brain clearing and activity mapping. Expression of the immediate early gene *c-fos* is used as a marker for cellular activation, since it is rapidly induced following a stimulus, readily immunolabeled in optically cleared brains, and spatially restricted to the cell nucleus giving high signal-to-noise for automated counting.

Experimental design and perfusion. Mice were injected with i.p. saline or nicotine and kept in a dim, quiet room for 1 h before perfusion to minimize off-target cFos expression. Mice were then perfused with 1× PBS followed by 20 ml of 4% paraformaldehyde (PFA, Electron Microscopy Services). Brains were carefully dissected from the skull and stored in PFA overnight. Brains were stored in PBS with 0.01% Sodium Azide (Sigma-Aldrich, Germany) until clearing.

iDISCO+ whole brain immunolabeling. Whole brain clearing and immunostaining was performed following the iDISCO+ protocol described previously [64] with minimal modifications. All the steps of the protocol were done at room temperature with gentle shaking unless otherwise specified. All the buffers were supplemented with 0.01% Sodium Azide (Sigma-Aldrich, Germany) to prevent bacterial and fungal growth. Briefly, perfused brains were dehydrated in an increasing series of methanol (Sigma-Aldrich, France) dilutions in water (washes of 1 h in methanol 20%, 40%, 60%, 80%, and 100%). An additional wash of 2 h in methanol 100% was done to remove residual water. Once dehydrated, samples were incubated overnight

in a solution containing a 66% dichloromethane (Sigma-Aldrich, Germany) in methanol, and then washed twice in methanol 100% (4 h each wash). Samples were then bleached overnight at 4°C in methanol containing a 5% of hydrogen peroxide (Sigma-Aldrich). Rehydration was done by incubating the samples in methanol 60%, 40%, and 20% (1 h each wash). After methanol pretreatment, samples were washed in PBS twice 15 min and 1 h in PBS containing a 0.2% of Triton X-100 (Sigma-Aldrich) and further permeabilized by a 24 h incubation at 37°C in permeabilization solution, composed by 20% dimethyl sulfoxide (Sigma-Aldrich), 2.3% Glycine (Sigma-Aldrich, USA) in PBS-T. In order to start the immunostaining, samples were first blocked with 0.2% gelatin (Sigma-Aldrich) in PBS-T for 24 h at 37°C, the same blocking buffer was used to prepare antibody solutions. Brains were incubated with anti c-Fos primary antibody (Synaptic systems 226–003) for 10 days at 37°C with gentle shaking, then washed in PBS-T (twice 1 h and then overnight), and finally newly incubated for 10 days with secondary antibodies. Secondary antibodies raised in donkeys, conjugated to Alexa 647 were used (Life Technologies). After immunostaining, the samples were washed in PBS-T (twice 1 h and then overnight), dehydrated in a methanol/water increasing concentration series (20%, 40%, 60%, 80%, 100% 1 h each and then methanol 100% overnight), followed by a wash in 66% dichloromethane—33% methanol for 3 h. Methanol was washed out with 2 final washes in dichloromethane 100% (15 min each) and finally the samples were cleared and stored in dibenzyl ether (Sigma-Aldrich) until light sheet imaging.

Light sheet microscopy. The acquisitions were done on a LaVision Ultramicroscope II equipped with infinity-corrected objectives. The microscope was installed on an active vibration filtration device, itself put on a marble compressed-air table. Imaging was done with the following filters: 595/40 for Alexa Fluor-555, and -680/30 for Alexa Fluor-647. The microscope was equipped with the following laser lines: OBIS-561nm 100mW, OBIS-639nm 70mW, and used the second generation LaVision beam combiner. The images were acquired with an Andor CMOS sNEO camera. Main acquisitions were done with the LVMI-Fluor 4X/O.3 WD6 LaVision Biotec objective. The microscope was connected to a computer equipped with SSD drives to speed up the acquisition. The brain was positioned in sagittal orientation, cortex side facing the light sheet, to maximize image quality and consistency. A field of view of $1,000 \times 1,300$ pixels was cropped at the center of the camera sensor. The light sheet numerical aperture was set to NA-0.03. The 3 light sheets facing the cortex were used, while the other side illumination was deactivated to improve the axial resolution. Beam width was set to the maximum. Laser powers were set to 40% to 60% (639 nm). The center of the light sheet in x was carefully calibrated to the center of the field. z steps were set to 6 mm. Tile overlaps were set to 10%. The whole acquisition took about 1 h per hemisphere. At the end of the acquisition, the objective was changed to a MI PLAN 1.1×/0.1 for the reference scan at 488 nm excitation (tissue autofluorescence). The field of view was cropped to the size of the brain, and the z-steps are set to 6 mm, and light sheet numerical aperture to 0.03 NA. It was important to crop the field of view to the size of the brain for subsequent alignment steps.

Computing resources. The data were automatically transferred every day from the acquisition computer to a Lustre server for storage. The processing with ClearMap was done on local workstations, either Dell Precision T7920 or HP Z840. Each workstation was equipped with 2 Intel Xeon Gold 6128 3.4G 6C/12T CPUs, 512Gb of 2666MHz DDR4 RAM, 4x1Tb NVMe Class 40 Solid State Drives in a RAID0 array (plus a separate system disk), and an NVIDIA Quadro P6000, 24Gb VRAM video card. The workstations were operated by Linux Ubuntu 20.04LTS. ClearMap 2.0 was used on Anaconda Python 3.7 environment.

ClearMap Fos+ cell counting. Tiled acquisitions of Fos-immunolabeled iDISCO+ cleared brains scanned with the light sheet microscope were processed with ClearMap 2 [49] to generate both voxel maps of c-Fos cell densities, as well as region-based statistics of cell counts.

Stitched images were processed for background removal, on which local maxima were detected to place initial seeds for the cells. A watershed was done on each seed to estimate the volume of the cell, and the cells were filtered according to their volume to exclude smaller artefactual maxima. The alignment of the brain to the Allen Brain Atlas was based on the acquired autofluorescence image using Elastix [65] (https://elastix.lumc.nl). Filtered cell's coordinates were transformed to their reference coordinate in the Allen Brain Atlas common coordinate system [66]. For voxel maps, spheres of 375 mm diameter were drawn on each filtered cell. *P*-value maps of significant differences between groups were generated using Mann–Whitney U test (SciPy implementation). Aligned voxelized data sets from each group of animals were manually inspected to identify the regional overlaps of *p*-value clusters, and volcano plots of regional counts were generated.

Decision model. Data choice (i.e., left or right) from all mice in the T-maze were modeled and fitted with a standard RL model [47]. The model uses the sequence of choices and outcomes (the reward) to estimate the expected value of each option for every trial. After each trial, the value associated with the chosen option was updated according to the classical delta rule: $V_R(t+1) = V_R(t) + \alpha\delta(t)$ and $\delta(t) = R_R(t) - V_R(t)$ where $\delta(t)$ is the reward prediction error (RPE), the difference between the expected value and the received reward, i.e., the RPE. $V_i = \{V_L, V_R\}$ is set to 1 when reward is water and 3 when reward is sucrose. For modeling, the expected values are set to zero at the beginning of the experiment. The learning rate α determines how rapidly the estimate of expected value is updated. Given expected values V_i for both options, the probability of choosing the right option $P_R(t)$ is computed using a SoftMax rule defined by $P_R(t) = 1/(1+\exp(-[\beta(V_R(t)-V_L(t)) + \chi(C_R(t-1)-C_L(t-1))]))$ with 2 parameters β and χ. The inverse temperature parameter β represents the sensitivity to the difference of values $V_i = \{V_L, V_R\}$, it reflects how much the difference in total value between the 2 options (ΔV) translates into more or less preference for the best option in a given gamble. With a small β, choices have low sensitivity for ΔV, with the extreme case of a null β where both options have the same probability to be selected. On the contrary, a large β indicates a high sensitivity to ΔV, with an infinite beta indicating that options associated with higher reward probabilities are always selected. The choice perseveration parameter χ captures short-term tendencies (previous choice) to perseverate or alternate (when positive or negative, respectively). This tendency to alternate is independent of the reward history [48], and thus does not depend on ΔV. The free parameters of the model (α, β, χ) were fitted by maximizing the data likelihood. Given a sequence of choice $c = c_{1...T}$, data likelihood is the product of their probability given by the SoftMax choice rule [67]. We used the optim function in R to perform the fits, with the constraints that $\alpha \in]0,1]$, $\beta \in]0,20]$, and $\chi \in [-2,2]$. For the simulation, the value of each option (left or right) is updated using the delta rule. The initial value associated with each option (before learning) is 1. The mice completed a succession of sessions consisting of 50 choices, with a specific reward value (V) associated with each side; V = 3 for sucrose, V = 1 for water or saccharine, V = 0.3 for nicotine (Fig 5F). For Fig 4D, ΔV varied from 3 to −1, with one side associated with a value of 1. At the end of each session, the reward position alternates. Each mouse is simulated with fitted values of β, χ, and α. Comparison (Bayesian information criterion and likelihood ratio test for nested model rule [67]) of the 3 parameters (α, β, χ) models with a classical 2 models (α, β) parameters indicated that the 3 parameters model provides the best fit for the data.

Statistical analysis. All statistical analyses were computed using R (The R Project, version 4.1.0) and Python with custom programs. Results were plotted as a mean ± SEM. The total number (*n*) of observations in each group and the statistics used are indicated in figure legends; *n* indicated number of mice and n_n number of cells (for electrophysiological recordings). Classical comparisons between means were performed using parametric tests (Student's *T* test,

or ANOVA for comparing more than 2 groups when parameters followed a normal distribution (Shapiro test $P > 0.05$) and nonparametric tests (here, Wilcoxon or Mann–Whitney) when the distribution was skewed. Multiple comparisons were corrected using a sequentially rejective multiple test procedure (Holm). Probability distributions were compared using the Kolmogorov–Smirnov (KS) test, and proportions were evaluated using a chi-squared test (χ^2). Regression was estimated using linear model and parameters a, R^2 and p in figures refer to the estimated slope, the adjusted R^2 correlation and the *p*-value for the slope estimation a. Matrix of Pearson's r correlation were estimated using rcorr function in Hmisc package (R). All statistical tests were two-sided. $P > 0.05$ was considered not to be statistically significant. For archetypal analysis, all computations and graphics have been done using the statistical software R and the archetype package (version 2.2–0.1). Briefly, the archetypal analysis finds the matrix Z of k m-dimensional archetypes (k is the number of archetypes), given an $n \times m$ matrix representing a multivariate data set with n observations (*n* = number of animals) and m attributes (here m = 5, consisting of the level of global switching (*Switch*), the variables *SwWat* and *SwSuc* that represent the probability of switching sides if the previous choice was water or sucrose, respectively, the *Pref* and *SideBias* that assess preference and side bias by comparing the choices (% of sucrose choice) between each session. Z is obtained by minimizing $\| X - \alpha Z^T \|_2$, with α the coefficients of the archetypes ($\alpha_{i,1..k} \geq 0$ and $\Sigma\alpha_{i,1..k} = 1$), and $\|.\|_2$ a matrix norm. The archetype is also a convex combination of the data points $Z = X^T\delta$ with $\delta \geq 0$ and their sum must be 1 [68]. The α-coefficient depicts the relative archetypal composition of a given observation. For k = 3, archetypes and an observation i, $\alpha_{i,1}; \alpha_{i,2}; \alpha_{i,3} \geq 0$ and $\alpha_{,1} + \alpha_{i,2} + \alpha_{i,3} = 1$. A ternary plot can then be used to visualize data. ($\alpha_{i,1}; \alpha_{i,2}; \alpha_{i,2}$) are used to assign individual behavior to its nearest archetype (i.e., k max($\alpha_{i,1}; \alpha_{i,2}; \alpha_{i,3}$)). $\alpha_{i,j}$ are also used as variable to estimate population archetypal composition. Archetypal composition correspond to α ($0 \leq \alpha_{i,j} \leq 1$). Pure archetype corresponds to 1, the archetypal composition decreases linearly with increasing distance from the archetype, 0 correspond to points on the opposite side.

Statistics and reproducibility.   All experiments were replicated with success.

Supporting information

S1 Fig. Comparison of the main environment variables depending on the archetype. Data are normalized to mean Tracker value (Tr). **(A)** variation in Occupancy, i.e., from left to right percent time in Nest compartment (%N), percent time in Food compartment (%F), percent time in Center compartment (%C), percent time in Stair compartment (%S), percent time in T-Maze compartment (%T). **(B)** First order probability transitions. *Inset*: Transitions of interest are labeled with a star. Center to Nest (CtoN), Center to Food (CtoF), Center to Stair (CtoS), Stair to T-maze (StoT). **(C)** Second order transition (probability): Nest to Stair (NtoS), Nest to Food (NtoF), Food to Stair (FtoS), Food to Nest (FtoN), Stair to Food (StoF), Stair to Nest (StoN). **(D)** Activity levels: Entropy (EnA), Number of Detections (NbD).
(TIFF)

S2 Fig. **(A)** Correlation (linear regression, a indicated the slope estimate, R^2 the Adjusted R-squared and p the *p*-value) between the mean number of T-maze entry per day (# nbtrial) and χ (*Top Left*), β (*Bottom*), and α (*Top right*) (n = 281 mice). **(B)** Comparison of the mean of 5 variable (*Switch*, *SwWat*, *SwSuc*, *Pref*, *SideBias*) for Tr, Ex, and NS archetype obtained for data (o) and for a model sequence (Δ) of 300 choices (6 sessions of 50 choices) simulated with fitted values of α, β, and χ. **(C)** Attribution study in which each of the latent variables is manipulated independently from the other to assess its contribution to the *Switch*, *SwWat*, *SwSuc*, *Pref*, *SideBias* variables, for the 3 archetypes. The legend symbols represent different simulation conditions. We modeled 6 sessions of 50 choices for the simulations, except for the last condition where the number of

choices was defined experimentally for each mouse. In this case, we defined the number of choices by taking the average number of trials per day for each mouse and multiplying it by 3 to represent 1 session of 3 days. Six such sessions were then used in the simulation. Empty circle: Each mouse is simulated using its estimated values of latent variables α, β and χ. Black circle: Each mouse is simulated with a random selection of latent variables α, β, and χ. Gray circle: Same as Black circle but with a number of trials/sessions estimated experimentally. White and Black circle: Each mouse is simulated with two of its estimated values and one is chosen randomly from the corresponding latent variables, respectively, α, β, or χ. **(D)** Percentage of Non-Switcher mice ($n = 52$) with a preferred side in WS session that correspond to: (white) same first sucrose choice side in WS session and same side preference in WW session, (blue) same first sucrose choice side in WS session and opposite side preference in WW session, (pink) opposite first sucrose choice side in WS session and same side preference in WW session and (light blue) opposite first sucrose choice side in WS session and opposite side preference in WW session.
(TIFF)

Acknowledgments

Author Contributions

Conceptualization: Sophie L. Fayad, Lauren M. Reynolds, Philippe Faure.

Formal analysis: Sophie L. Fayad, Lauren M. Reynolds, Robin Justo, Steve Didienne, Nicolas Debray, Yasmine Layadi, Philippe Faure.

Funding acquisition: Philippe Faure.

Investigation: Sophie L. Fayad, Lauren M. Reynolds, Nicolas Torquet, Stefania Tolu, Sarah Mondoloni, Claire Nguyen, Amy Siriphanh, Cécile Viollet, Louis Raynaud, Coralie Fouquet, Bernadette Hannesse, Ana-Marta Capaz, Thomas Topilko, Fabio Marti.

Methodology: Sophie L. Fayad, Lauren M. Reynolds, Nicolas Torquet, Nicolas Renier, Fabio Marti, Philippe Faure.

Supervision: Nicolas Renier, Alexandre Mourot, Fabio Marti, Philippe Faure.

Validation: Sophie L. Fayad, Lauren M. Reynolds, Nicolas Renier, Alexandre Mourot, Fabio Marti, Philippe Faure.

Writing – original draft: Sophie L. Fayad, Lauren M. Reynolds, Cécile Viollet, Alexandre Mourot, Fabio Marti, Philippe Faure.

Writing – review & editing: Lauren M. Reynolds, Nicolas Torquet, Stefania Tolu, Sarah Mondoloni, Claire Nguyen, Amy Siriphanh, Robin Justo, Steve Didienne, Nicolas Debray, Cécile Viollet, Louis Raynaud, Yasmine Layadi, Coralie Fouquet, Bernadette Hannesse, Ana-Marta Capaz, Thomas Topilko, Nicolas Renier, Alexandre Mourot, Fabio Marti, Philippe Faure.

References

1. Sih A, Bell AM, Johnson JC, Ziemba RE. Behavioral Syndromes: An Integrative Overview. Q Rev Biol. 2004; 79:241–277. https://doi.org/10.1086/422893 PMID: 15529965

2. Bergmüller R, Taborsky M. Animal personality due to social niche specialisation. Trends Ecol Evol. 2010; 25:504–511. https://doi.org/10.1016/j.tree.2010.06.012 PMID: 20638151

3. Kempermann G. Environmental enrichment, new neurons and the neurobiology of individuality. Nat Rev Neurosci. 2019; 78:1–11. https://doi.org/10.1038/s41583-019-0120-x PMID: 30723309

4. Pennisi E. The power of personality. Science. 2016; 352:644–647. https://doi.org/10.1126/science.352.6286.644 PMID: 27151848

5. Torquet N, Marti F, Campart C, Tolu S, Nguyen C, Oberto V, et al. Social interactions impact on the dopaminergic system and drive individuality. Nat Commun. 2018; 9:3081. https://doi.org/10.1038/s41467-018-05526-5 PMID: 30082725

6. Zilkha N, Chuartzman SG, Sofer Y, Pen Y, Cum M, Mayo A, et al. Sex-dependent control of phero-mones on social organization within groups of wild house mice. Curr Biol. 2023. https://doi.org/10.1016/j.cub.2023.02.039 PMID: 36917976

7. Sofer Y, Zilkha N, Gimpel E, Wagner S, Chuartzman SG, Kimchi T. Sexually dimorphic oxytocin circuits drive intragroup social conflict and aggression in wild house mice. Nat Neurosci. 2024;1–9. https://doi.org/10.1038/s41593-024-01685-5 PMID: 38969756

8. Deroche-Gamonet V, Belin D, Piazza PV. Evidence for addiction-like behavior in the rat. Science (New York, NY). 2004; 305:1014–1017. https://doi.org/10.1126/science.1099020 PMID: 15310906

9. Freund J, Brandmaier AM, Lewejohann L, Kirste I, Kritzler M, Kruger A, et al. Emergence of Individuality in Genetically Identical Mice. Science (New York, NY). 2013; 340:756–759. https://doi.org/10.1126/science.1235294 PMID: 23661762

10. Faure P, Fayad SL, Solié C, Reynolds LM. Social Determinants of Inter-Individual Variability and Vul-nerability: The Role of Dopamine. Front Behav Neurosci. 2022; 16:836343. https://doi.org/10.3389/fnbeh.2022.836343 PMID: 35386723

11. Weissbrod A, Shapiro A, Vasserman G, Edry L, Dayan M, Yitzhaky A, et al. Automated long-term track-ing and social behavioural phenotyping of animal colonies within a semi-natural environment. Nature IDAA Commun. 2013;4. https://doi.org/10.1038/ncomms3018 PMID: 23771126

12. Zilkha N, Sofer Y, Beny Y, Kimchi T. From classic ethology to modern neuroethology: overcoming the three biases in social behavior research. Curr Opin Neurobiol. 2016; 38:96–108. https://doi.org/10.1016/j.conb.2016.04.014 PMID: 27179302

13. Hayden BY. Economic choice: the foraging perspective. Curr Opin Behav Sci. 2018; 24:1–6. https://doi.org/10.1016/j.cobeha.2017.12.002

14. Hayden BY, Walton ME. Neuroscience of foraging. Front Neurosci. 2014; 8:81. https://doi.org/10.3389/fnins.2014.00081 PMID: 24795556

15. Mobbs D, Trimmer PC, Blumstein DT, Dayan P. Foraging for foundations in decision neuroscience: insights from ethology. Nat Rev Neurosci. 2018; 19:419–427. https://doi.org/10.1038/s41583-018-0010-7 PMID: 29752468

16. Timberlake W, Peden BF. On the distinction between open and closed economies. J Exp Anal Behav. 1987; 48:35–60. https://doi.org/10.1901/jeab.1987.48-35 PMID: 3625103

17. Rowland NE, Vaughan CH, Mathes CM, Mitra A. Feeding behavior, obesity, and neuroeconomics. Phy-siol Behav. 2008; 93:97–109. https://doi.org/10.1016/j.physbeh.2007.08.003 PMID: 17825853

18. Beeler JA, Daw N, Frazier CRM, Zhuang X. Tonic dopamine modulates exploitation of reward learning. Front Behav Neurosci. 2010; 4:170. https://doi.org/10.3389/fnbeh.2010.00170 PMID: 21120145

19. Gartland LA, Firth JA, Laskowski KL, Jeanson R, Ioannou CC. Sociability as a personality trait in ani-mals: methods, causes and consequences. Biol Rev. 2021. https://doi.org/10.1111/brv.12823 PMID: 34894041

20. Skóra MN, Pattij T, Beroun A, Kogias G, Mielenz D, de Vries T, et al. Personality driven alcohol and drug abuse: New mechanisms revealed. Neurosci Biobehav Rev. 2020; 116:64–73. https://doi.org/10.1016/j.neubiorev.2020.06.023 PMID: 32565173

21. Kreek MJ, Nielsen DA, Butelman ER, LaForge KS. Genetic influences on impulsivity, risk taking, stress responsivity and vulnerability to drug abuse and addiction. Nat Neurosci. 2005; 8:1450–1457. https://doi.org/10.1038/nn1583 PMID: 16251987

22. Diergaarde L, Pattij T, Poortvliet I, Hogenboom F, de Vries W, Schoffelmeer ANM, et al. Impulsive choice and impulsive action predict vulnerability to distinct stages of nicotine seeking in rats. Biol Psy-chiatry. 2008; 63:301–308. https://doi.org/10.1016/j.biopsych.2007.07.011 PMID: 17884016

23. Perkins KA, Lerman C, Coddington SB, Jetton C, Karelitz JL, Scott JA, et al. Initial nicotine sensitivity in humans as a function of impulsivity. Psychopharmacology (Berl). 2008; 200:529–544. https://doi.org/10.1007/s00213-008-1231-7 PMID: 18604520

24. Perkins KA, Gerlach D, Broge M, Grobe JE, Wilson A. Greater sensitivity to subjective effects of nicotine in nonsmokers high in sensation seeking. Exp Clin Psychopharmacol. 2000; 8:462–471. https://doi.org/10.1037//1064-1297.8.4.462 PMID: 11127418

25. Addicott MA, Pearson JM, Sweitzer MM, Barack DL, Platt ML. A Primer on Foraging and the Explore/Exploit Trade-Off for Psychiatry Research. Neuropsychopharmacology. 2017; 42:1931–1939. https://doi.org/10.1038/npp.2017.108 PMID: 28553839

26. Berke JD. What does dopamine mean? Nat Neurosci. 2018; 21:787–793. https://doi.org/10.1038/s41593-018-0152-y PMID: 29760524

27. Schultz W. Multiple dopamine functions at different time courses. Annu Rev Neurosci. 2007; 30:259–288. https://doi.org/10.1146/annurev.neuro.28.061604.135722 PMID: 17600522

28. Solié C, Girard B, Righetti B, Tapparel M, Bellone C. VTA dopamine neuron activity encodes social interaction and promotes reinforcement learning through social prediction error. Nat Neurosci. 2021;1–12. https://doi.org/10.1038/s41593-021-00972-9 PMID: 34857949

29. Exley R, Maubourguet N, David V, Eddine R, Evrard A, Pons S, et al. Distinct contributions of nicotinic acetylcholine receptor subunit alpha4 and subunit alpha6 to the reinforcing effects of nicotine. Proc Natl Acad Sci U S A. 2011; 108:7577–7582. https://doi.org/10.1073/pnas.1103000108 PMID: 21502501

30. Maskos U, Molles BE, Pons S, Besson M, Guiard BP, Guilloux J-P, et al. Nicotine reinforcement and cognition restored by targeted expression of nicotinic receptors. Nature. 2005; 436:103–107. https://doi.org/10.1038/nature03694 PMID: 16001069

31. Mameli-Engvall M, Evrard A, Pons S, Maskos U, Svensson TH, Changeux J-P, et al. Hierarchical control of dopamine neuron-firing patterns by nicotinic receptors. Neuron. 2006; 50:911–921. https://doi.org/10.1016/j.neuron.2006.05.007 PMID: 16772172

32. Morel C, Fattore L, Pons S, Hay YA, Marti F, Lambolez B, et al. Nicotine consumption is regulated by a human polymorphism in dopamine neurons. Mol Psychiatry. 2014; 19:930–936. https://doi.org/10.1038/mp.2013.158 PMID: 24296975

33. Faure P, Tolu S, Valverde S, Naudé J. Role of nicotinic acetylcholine receptors in regulating dopamine neuron activity. Neuroscience. 2014; 282C:86–100. https://doi.org/10.1016/j.neuroscience.2014.05.040 PMID: 24881574

34. Naudé J, Dongelmans M, Faure P. Nicotinic alteration of decision-making. Neuropharmacology. 2015; 96:244–254. https://doi.org/10.1016/j.neuropharm.2014.11.021 PMID: 25498234

35. Maubourguet N, Lesne A, Changeux J-P, Maskos U, Faure P. Behavioral sequence analysis reveals a novel role for beta2* nicotinic receptors in exploration. Friston KJ, editor. PLoS Comput Biol. 2008; 4:e1000229. https://doi.org/10.1371/journal.pcbi.1000229 PMID: 19023420

36. Addicott MA, Pearson JM, Wilson J, Platt ML, McClernon FJ. Smoking and the bandit: A preliminary study of smoker and nonsmoker differences in exploratory behavior measured with a multiarmed bandit task. Exp Clin Psychopharmacol. 2013; 21:66–73. https://doi.org/10.1037/a0030843 PMID: 23245198

37. Sidorenko N, Chung H-K, Grueschow M, Quednow BB, Hayward-Könnecke H, Jetter A, et al. Acetylcholine and noradrenaline enhance foraging optimality in humans. Proc Natl Acad Sci U S A. 2023; 120:e2305596120. https://doi.org/10.1073/pnas.2305596120 PMID: 37639601

38. Dongelmans M, Cuttoli RD, Nguyen C, Come M, Duranté EK, Lemoine D, et al. Chronic nicotine increases midbrain dopamine neuron activity and biases individual strategies towards reduced exploration in mice. Nat Commun. 2021; 12:6945. https://doi.org/10.1038/s41467-021-27268-7 PMID: 34836948

39. Barik J, Marti F, Morel C, Fernandez SP, Lanteri C, Godeheu G, et al. Chronic stress triggers social aversion via glucocorticoid receptor in dopaminoceptive neurons. Science (New York, NY). 2013; 339:332–335. https://doi.org/10.1126/science.1226767 PMID: 23329050

40. Chaudhury D, Walsh JJ, Friedman AK, Juarez B, Ku SM, Koo JW, et al. Rapid regulation of depression-related behaviours by control of midbrain dopamine neurons. Nature. 2013; 493:532 536. https://doi.org/10.1038/nature11713 PMID: 23235832

41. Morel C, Fernandez SP, Pantouli F, Meye FJ, Marti F, Tolu S, et al. Nicotinic receptors mediate stress-nicotine detrimental interplay via dopamine cells' activity. Mol Psychiatry. 2017; 23:1597–1605. https://doi.org/10.1038/mp.2017.145 PMID: 29155800

42. Pomerleau OF. Individual differences in sensitivity to nicotine: Implications for genetic research on nicotine dependence. Behav Genet. 1995; 25:161–177. https://doi.org/10.1007/BF02196925 PMID: 7733857

43. Mondoloni S, Nguyen C, Vicq E, Jehl J, Cuttoli RD, Torquet N, et al. Prolonged nicotine exposure reduces aversion to the drug in mice by altering nicotinic transmission in the interpeduncular nucleus. Biorxiv. 2022;2021.12.16.472949. https://doi.org/10.1101/2021.12.16.472949

44. Faure P, Neumeister H, Faber DS, Korn H. Symbolic analysis of swimming trajectories reveals scale invariance and provides a model for fish locomotion. World Scientific. 2003; 11:233–243.

45. Cutler A, Breiman L. Archetypal Analysis. Dent Tech. 1994; 36:338–347. https://doi.org/10.2307/1269949

46. Hart Y, Sheftel H, Hausser J, Szekely P, Ben-Moshe NB, Korem Y, et al. Inferring biological tasks using Pareto analysis of high-dimensional data. Nat Methods. 2015; 12:233–5–3 p following 235. https://doi.org/10.1038/nmeth.3254 PMID: 25622107

47. Sutton RS, Barto AG. Reinforcement Learning. MIT Press; 1998.

48. Rutledge RB, Lazzaro SC, Lau B, Myers CE, Gluck MA, Glimcher PW. Dopaminergic drugs modulate learning rates and perseveration in Parkinson's patients in a dynamic foraging task. J Neurosci. 2009; 29:15104–15114. https://doi.org/10.1523/JNEUROSCI.3524-09.2009 PMID: 19955362

49. Renier N, Adams EL, Kirst C, Wu Z, Azevedo R, Kohl J, et al. Mapping of Brain Activity by Automated Volume Analysis of Immediate Early Genes. Cell. 2016; 165:1789–1802. https://doi.org/10.1016/j.cell.2016.05.007 PMID: 27238021

50. Pich EM, Chiamulera C, Tessari M. Neural substrate of nicotine addiction as defined by functional brain maps of gene expression. J Physiol-Paris. 1998; 92:225–228. https://doi.org/10.1016/s0928-4257(98)80015-6 PMID: 9789813

51. Pagliusi SR, Tessari M, DeVevey S, Chiamulera C, Pich EM. The Reinforcing Properties of Nicotine are Associated with a Specific Patterning of c-fos Expression in the Rat Brain. Eur J Neurosci. 1996; 8:2247–2256. https://doi.org/10.1111/j.1460-9568.1996.tb01188.x PMID: 8950089

52. Eddine R, Valverde S, Tolu S, Dautan D, Hay A, Morel C, et al. A concurrent excitation and inhibition of dopaminergic subpopulations in response to nicotine. Sci Rep. 2015; 5:8184. https://doi.org/10.1038/srep08184 PMID: 25640814

53. Nguyen C, Mondoloni S, Borgne TL, Centeno I, Come M, Jehl J, et al. Nicotine inhibits the VTA-to-amygdala dopamine pathway to promote anxiety. Neuron. 2021. https://doi.org/10.1016/j.neuron.2021.06.013 PMID: 34242565

54. Gomez-Marin A, Ghazanfar AA. The Life of Behavior. Neuron. 2019; 104:25–36. https://doi.org/10.1016/j.neuron.2019.09.017 PMID: 31600513

55. Lopes JB, Senko AN, Bahnsen K, Geisler D, Kim E, Bernanos M, et al. Individual behavioral trajectories shape whole-brain connectivity in mice. Biorxiv. 2022;2022.03.25.485806. https://doi.org/10.1101/2022.03.25.485806

56. Markowitz JE, Gillis WF, Jay M, Wood J, Harris RW, Cieszkowski R, et al. Spontaneous behaviour is structured by reinforcement without explicit reward. Nature. 2023;1–10. https://doi.org/10.1038/s41586-022-05611-2 PMID: 36653449

57. Coddington LT, Lindo SE, Dudman JT. Mesolimbic dopamine adapts the rate of learning from action. Nature. 2023;1–9. https://doi.org/10.1038/s41586-022-05614-z PMID: 36653450

58. Dember WN, Fowler H. Spontaneous alternation behavior. Psychol Bull. 1958; 55:412–428. PMID: 13602020

59. Sandi C. Understanding the neurobiological basis of behavior: a good way to go. Front Neurosci. 2008; 2:129–130. https://doi.org/10.3389/neuro.01.046.2008 PMID: 19225579

60. Schaefer AT, Claridge-Chang A. The surveillance state of behavioral automation. Curr Opin Neurobiol. 2012; 22:170–176. https://doi.org/10.1016/j.conb.2011.11.004 PMID: 22119142

61. Spruijt BM, DeVisser L. Advanced behavioural screening: automated home cage ethology. Drug Discov Today Technol. 2006; 3:231–237. https://doi.org/10.1016/j.ddtec.2006.06.010 PMID: 24980412

62. Castelhano-Carlos M, Costa PS, Russig H, Sousa N. PhenoWorld: a new paradigm to screen rodent behavior. Transl Psychiatry. 2014; 4:e399–11. https://doi.org/10.1038/tp.2014.40 PMID: 26126181

63. Ungless MA, Grace AA. Are you or aren't you? Challenges associated with physiologically identifying dopamine neurons. Trends Neurosci. 2012; 35:422–430. https://doi.org/10.1016/j.tins.2012.02.003 PMID: 22459161

64. Renier N, Wu Z, Simon DJ, Yang J, Ariel P, Tessier-Lavigne M. iDISCO: A Simple, Rapid Method to Immunolabel Large Tissue Samples for Volume Imaging. Cell. 2014; 159:896–910. https://doi.org/10.1016/j.cell.2014.10.010 PMID: 25417164

65. Klein S, Staring M, Murphy K, Viergever MA, Pluim JPW. elastix: a toolbox for intensity-based medical image registration. IEEE Trans Méd Imaging. 2009; 29:196–205. https://doi.org/10.1109/TMI.2009.2035616 PMID: 19923044

66. Wang Q, Ding S-L, Li Y, Royall J, Feng D, Lesnar P, et al. The Allen Mouse Brain Common Coordinate Framework: A 3D Reference Atlas. Cell. 2020; 181:936–953.e20. https://doi.org/10.1016/j.cell.2020.04.007 PMID: 32386544

67. Daw ND. Trial-by-trial data analysis using computational models. Decision Making, Affect, and Learning. Oxford University Press; 2011. p. 3–38. https://doi.org/10.1093/acprof:oso/9780199600434.003.0001

68. Eugster MJA, Leisch F. From Spider-Man to Hero—Archetypal Analysis in R. J Stat Softw. 2009; 30:1–23. https://doi.org/10.18637/jss.v030.i08